RESEARCH ARTICLE

Extracellular vesicles from lung tissue drive bone marrow neutrophil recruitment in inflammation

Bowen Liu[1] | Yuan Jin[1] | Jingyi Yang[1] | Yue Han[1] | Hui Shan[2] | Mantang Qiu[3] | Xuyang Zhao[1] | Anhang Liu[1] | Yan Jin[1] | Yuxin Yin[1,2]

[1]Institute of Systems Biomedicine, Department of Pathology, Beijing Key Laboratory of Tumour Systems Biology, School of Basic Medical Sciences, Peking-Tsinghua Center for Life Sciences, Peking University Health Science Center, Beijing, China

[2]Institute of Precision Medicine, Peking University Shenzhen Hospital, Shenzhen, China

[3]Department of Thoracic Surgery, Peking University People's Hospital, Beijing, China

Correspondence
Yuxin Yin, Institute of Systems Biomedicine, School of Basic Medical Sciences, Peking University Health Science Center, 38 Xueyuan Road, Haidian, Beijing 100191, China.
Email: yinyuxin@bjmu.edu.cn

Abstract
Extracellular vesicles (EVs) are single-membrane vesicles that play an essential role in long-range intercellular communications. EV investigation has been explored largely through cell-culture systems, but it remains unclear how physiological EVs exert homeostatic or pathological functions in vivo. Here, we report that lung EVs promote chemotaxis of neutrophils in bone marrow through delivery of double stranded DNA (dsDNA). We have identified and characterized EVs containing dsDNA collected from both human and murine lung tissues using newly developed approaches. Our analysis of EV proteomics together with single-cell RNA sequencing data reveals that type II alveolar epithelial cells are the main source of the lung EVs. Furthermore, we demonstrate that the lung EVs accumulate in bone marrow and enhance neutrophil recruitment under inflammation conditions. Moreover, lung EV-DNA stimulates neutrophils to release the chemokines CXCL1 and CXCL2 via DNA-TLR9 signalling. Our findings establish a molecular basis of lung EVs in enhancement of host immune response to bacterial infection and provide new insights into understanding of vesicle-mediated systematic communications.

KEYWORDS
dsDNA, lung EVs, neutrophil chemotaxis

1 | INTRODUCTION

Extracellular vesicles (EVs) are increasingly being recognized as biomarkers of diseases and as vectors of long-range intercellular communications in the body (Shao et al., 2018). Based on their biochemical and biophysical characteristics as well as subcellular origin, EVs are classified into microvesicles, apoptotic bodies and exosomes (Andaloussi et al., 2013). EVs have emerged as a novel messaging system of the organism, mediating cell-cell and interorgan communications, as well as maintaining homeostasis and health in multicellular organisms (Tkach & Thery, 2016; Verweij et al., 2019).

Most studies to date have utilized EVs isolated from cell culture media (Gardiner et al., 2016; Lima et al., 2009). However, cultured cells lack the influence of other cell types that co-exist in a physiological microenvironment. Studies focusing on EVs isolated directly from tissues are expected to provide more relevant information; however, techniques for EV isolation from intact tissues are currently suboptimal. The lung is a complex organ directly connected to the external environment and plays critical roles in gas exchange, oxidative metabolism, and maintenance of immune homeostasis. Besides, the lung has communications with other anatomically distinct organs, like gut and kidney (Enaud et al., 2020; Faubel & Edelstein, 2016; Herrlich, 2021; Merk et al., 2021; Shashaty et al., 2019). It also has been reported that lung tumours can remotely activate osteoblastic cells in bones

---

Bowen Liu and Yuan Jin contributed equally to this work.

even in the absence of local metastasis and induced Siglec-F^{high} neutrophils from bone marrow to promote tumour growth (Engblom et al., 2017). In addition, lung derived EVs can be internalized by bone marrow cells in vitro (Aliotta et al., 2012, 2015). These findings indicate that the lung is a sophisticated organ that has untapped potential cross-talk with other organs. However, our understanding of routes and mediators in interorgan communications remains limited. Therefore, it is important to establish reliable and validated methods to collect EVs from lung tissues according to their distinctive properties, to yield valuable information regarding physiological characteristics and remote regulatory roles of lung EVs, as well as to identify unknown mechanisms of interorgan communications between the lung and other organs.

EV cargoes are diverse and include both proteins and nucleic acids (Jeppesen et al., 2019; Skotland et al., 2017). Several studies have reported that EVs do contain DNA, including single-stranded DNA, double-stranded (ds) DNA, genomic DNA, as well as mitochondrial DNA (Balaj et al., 2011; Li et al., 2013; Sansone et al., 2017; Thakur et al., 2014; Yokoi et al., 2019). EV-based DNA secretion is proposed to contribute to cellular homeostasis and attenuation of mitochondrial damage by excreting harmful DNA from cells (Takahashi et al., 2017; Zhao et al., 2021), and may be a useful diagnostic tumour biomarker (Thakur et al., 2014; Wang et al., 2018). However, other studies have reported that extracellular DNA is secreted through an autophagy- and MVE-dependent but exosome-independent mechanism (Jeppesen et al., 2019). Clearly, further investigation is needed to better understand the role of EVs in DNA secretion.

Here, we have established an effective method to collect high-quality EVs from human and murine lung tissues. The vesicles were rigorously characterized and defined as EVs based on their size, morphology, density and proteomic contents, fulfilling the experimental requirements of EVs as proposed by the International Society for Extracellular Vesicles (Lötvall et al., 2014). Analysis of lung EV proteomics combined with single-cell RNA sequencing (scRNA-seq) data showed that the main source of lung EVs was type II alveolar epithelial (ATII) cells. Furthermore, we confirmed that dsDNA exists both inside and outside of lung EVs. The function of lung EVs in long-distance transport was then examined and we found that they specifically accumulated in the bone marrow in vivo and promoted chemoattractant-induced migration of neutrophils. Finally, we demonstrated that dsDNA derived from lung EVs could be sensed by toll-like receptor 9 (TLR9) which in turn induced CXCL1 and CXCL2 expression in neutrophils, leading to enhanced chemotaxis. We conclude that lung EVs contain both protein and dsDNA components which play critical roles in neutrophil recruitment during the early phase of bacterial infection.

2 | MATERIALS AND METHODS

2.1 | Human samples

Fresh lung tissues were resected from patients undergoing a lobectomy for focal lung tumours in the Department of Thoracic Surgery, Peking University People's Hospital. Normal lung tissues were obtained from uninvolved regions greater than 5 cm from the edge of the tumours. None of the patients included in this study had undergone any preoperative radiation or chemotherapy. All procedures were conducted under the approval of the Ethics Committee of Peking University People's Hospital (No. 2021PHB118-001), and informed patient consent was obtained from all subjects in advance of sample collection.

2.2 | Mice

C57BL/6 mice, BALB/c mice and *ROSA26-CAG-LSL-tdTOMATO* mice (B6. Cg-*Gt(ROSA)26Sor*$^{tm9\ (CAG-tdTomato)\ Hze}$ /J) were purchased from Beijing Vitalstar Biotechnology Co., Ltd. All mice were kept in a special pathogen-free facility at PKU Care Industrial Park, and were used for experiments at age 6–8 weeks. All procedures were approved and monitored by the Animal Care and Use Committee of Peking University.

2.3 | Cell lines

HECV cell line was obtained from Interlab Cell Line Collection (ICLC) and other cell lines used in this work were obtained from the American Type Culture Collection (ATCC). HEK293T, A549, HECV and LLC cell lines were cultured in DMEM (Gibco) supplemented with 10% FBS and 1% penicillin/streptomycin. NCI-H1299, HCC827, Raji, K562 and Jurkat cell lines were cultured in RPMI-1640 medium (Gibco) supplemented with 10% FBS and 1% penicillin/streptomycin. All cultured cells were incubated at 37°C, 5 % CO$_2$. All human cell lines have been authenticated by STR (short tandem repeat) profiling.

2.4 | Isolation of EVs from cultured cells

Growth medium used for EV collection was prepared with 10% FBS and ultracentrifuged at 110,000 × g for 18 h at 4°C to remove EVs in FBS. After 48 h of culture, EVs from cell-conditioned medium were extracted by a standard differential centrifugation

protocol. In brief, cell-conditioned medium was serially centrifuged at $300 \times g$ for 20 min, $3000 \times g$ for 20 min and $10,000 \times g$ for 60 min at 4°C to remove cells, debris and large vesicles. The supernatant was passed through 0.22 μm pore PES filters (Millipore) and then centrifuged at $110,000 \times g$ for 70 min at 4°C to pellet EVs. Subsequently, EVs were washed once and finally resuspended using PBS.

2.5 | Isolation of EVs from lung tissues

According to the characteristics of lung tissues, we established an effective method to collect EVs from murine or human lung tissues.

Enzymatic digestion of murine lung tissues was performed as described by Marcus Gereke et al. (Gereke et al., 2012). Briefly, the mouse was sacrificed by CO_2 asphyxiation, and the lung was perfused with pre-chilled PBS until free of blood. After exposure of the trachea, a smoothed 2 ml syringe needle was inserted into the trachea and followed by fixation. Around 2 ml dispase II working solution (Roche, 3 U/ml) was instilled through the needle until all lobes were fully expanded. Around 0.6 ml liquefied 1% agarose (shortly heat to 95°C until liquefied and cool to 45°C until use) was subsequently instilled. After the agarose gelled, the lung was excised and transferred into 2 ml dispase II working solution and incubated at room temperature for 1 h.

Human lung tissue masses (>500 mg) were placed in pre-chilled tissue storage solution (MACS) and kept on ice (or 4°C) for less than 12 h before the lung EVs extraction process began. During digestion, tissue masses were transferred into dispase II working solution (1 ml per 100 mg lung tissue). The lung tissue masses were gently cut into pieces by a sterile ophthalmic scissors until all pieces have a homogeneous size of approximately $2 \times 2 \times 2$ mm and were then digested at 37°C for 1 h.

After dispase II digestion, the lung tissue suspension of human or mouse was transferred into a petri dish containing 10 ml RPMI-1640 medium containing 0.5 mg/ml DNase I (Sigma Aldrich) and further disintegrated by blunt dissection. After dispersing on a shaker at room temperature for 20 min, the cell suspension was filtered through a nylon cell strainer (FALCON) with 100 μm pores followed by serial centrifugations at $300 \times g$ for 20 min, $3000 \times g$ for 20 min and $10,000 \times g$ for 60 min at 4°C to remove cells, debris and large vesicles. The supernatant was passed through a 0.22 μm pore PES filter (Millipore) and next subjected to ultracentrifugation at $110,000 \times g$ for 70 min at 4°C in a 45Ti rotor (Beckman Coulter) to sediment EVs. The pellets were resuspended in PBS for washing and centrifuged at $110,000 \times g$ in a 45Ti rotor (Beckman Coulter) and a TLA-55 Rotor (Beckman Coulter) for 70 min in turn. Finally, the pellets (crude EVs) were resuspended in 30 μl PBS.

Ten-layers sucrose density gradient centrifugation was then performed for EVs purification. Briefly, 0.45 ml 2.5 M sucrose solution was firstly poured to the bottom of an MLS-50 centrifuge tube. The crude EVs were resuspended in 0.45 ml 2.25 M sucrose solution and then poured on the top of 2.5 M sucrose. Layers of 2 M, 1.75 M, 1.5 M, 1.25 M, 1 M, 0.75 M, 0.5 M and 0.25 M sucrose solution (0.45 ml for each layer) were then subsequently poured in turn. The gradients were ultracentrifuged at $180,000 \times g$ for 13 h at 4°C, in an MLS-50 swinging-bucket rotor (Beckman Coulter), and then ten fractions were collected. Each fraction was mixed with 0.9 ml PBS for dilution followed by ultracentrifugation at $110,000 \times g$ for 70 min at 4°C. The pellets from low-density fractions (F1–F5) were collected as lung EVs and the pellets from high-density fractions (F6–F10) were collected as non-vesicular components. All the pellets were resuspended in 50–100 μl PBS for subsequent experiments.

2.6 | Transmission electron microscopy (TEM)

In order to adsorb sufficient lung EVs, glow-discharged copper grids were floated on a suspension of lung EVs fixed with 2.5% glutaraldehyde.

For fresh lung tissues from mice, tissues were fixed with 2.5% glutaraldehyde and then treated with 1% OsO4 for 2 h followed by dehydration with a graded series of ethanol (50%, 70%, 90%, 95%, and 100%). Subsequently, ultrathin sections (50 nm) of the fixed lung tissues were cut with an ultra-microtome (Leica EM UC-7) and loaded onto glow-discharged copper grids.

All samples were then negatively stained with 2% uranyl acetate, and examined with a JEM-1400 transmission electron microscope (JEOL Ltd., Japan).

2.7 | Cryo-electron microscopy

Lung EVs were examined using a cryo-electron microscope (Talos Arctica Cryo-TEM; Thermo Fisher). Quantifoil 1.2/1.3 copper grids were firstly glow discharged (30 mA, 60 s) and then loaded with lung EV samples prepared using a FEI Vitrobot Mark IV system. The grids were observed for data collection using 105 kx magnification and a total dose of 50 $e^-/\text{Å}^2$.

2.8 | Nanoparticle tracking analysis (NTA)

The concentration and size distribution profiles of EVs were determined on a NanoSight NS300 instrument (Malvern, UK) equipped with a Blue 405 nm laser and a sCMOS camera. Samples were diluted 1:100 in 0.22 μm filtered PBS to achieve 20–100 particles per field of view. EVs were injected into the sample-carrier cell, and the particles were automatically tracked and sized based on Brownian motion and the diffusion coefficient. The size distribution and particle concentration each represent the mean of three individual measurements with acquisition time of 60 s with a camera level setting at 12 and at the temperature of 25°C ± 0.5°C. After capture, the videos were analysed using NTA 3.3 Dev Build 3.3.104 software with a detection threshold five.

2.9 | EV fluorescence labelling

Labelling of EVs with fluorescent lipophilic tracer DiR/DiI (AAT Bioquest, 5 μM), DAPI (Beyotime, 10 μg/ml) and SYTOX (Thermo Fisher, 1 μM) was performed according to the manufacturer's protocols. Briefly, EVs were diluted in PBS prior to addition of the dyes. Labelling was performed for 20 min at room temperature in the dark and terminated using 0.1% BSA (Sigma Aldrich) in PBS. EVs were centrifuged at 110,000 × g for 70 min to remove any remaining free dye, resuspended in PBS and then transferred into recipient mice.

2.10 | Confocal microscopy

Murine bone marrow cells were cultured on glass slides, and fixed with 4% paraformaldehyde for 30 min. Cells were then permeabilized with 0.5% Triton X-100 (Sigma Aldrich) for 10 min at room temperature, followed by blocking with 1% BSA and incubation with specific primary antibodies. After incubation with fluorescent secondary antibodies (Alexa Fluor 488 and 555, Invitrogen), coverslips were mounted and assessed by fluorescence microscopy. Images were acquired using a Nikon TCS A1 microscope.

Other samples were analysed under a Leica TCS SP8 DIVE (Deep In Vivo Explorer) confocal microscope. To observe fluorescent labelled EVs, an APO 63 × oil lens (NA 1.4) was used and images processed by deconvolution calculation. Intravital imaging of mouse lung tissues was achieved by two-photon laser scanning microscopy, using an APO 25 × water lens (NA 0.95). Mice were intranasally treated with DiI-labelled lung EVs, and 24 h later, FITC-dextran (70 kDa) was injected intravenously 20 min before sacrifice to label blood vessels. Care was taken to ensure fresh mouse lung tissue could be observed within 30 min ex vivo.

2.11 | In vivo imaging

Male BALB/c mice (6–8 weeks) were intravenously injected with DiR-labelled lung EVs. At 48 h post administration, each mouse was anesthetized with 2.5% Avertin and imaged using a Lumina XR imaging system. In addition, freshly removed femurs were further imaged using the same imaging system. Excitation and emission wavelength were set at 780 nm and 845 nm, respectively.

2.12 | Mass spectrometry

Lung EVs (40 μg in PBS) and lung cell lysates (40 μg) were analysed by LC–MS/MS, as previously described (Lu et al., 2015). The collected lung EVs were lysed with RIPA lysis buffer (50 mM Tris-HCl (pH 7.4), 150 mM NaCl, 1% NP-40, 1% sodium deoxycholate and 0.1% SDS) containing protease inhibitors. Mass spectra data were acquired with an LTQ Orbitrap Elite mass spectrometer (Thermo Fisher) equipped with a nanoelectrospray ion source (Proxeon Biosystems). Fragmentation was performed by collision-induced dissociation (normalized collision energy, 35%; activation Q, 0.250; activation time, 10 ms) with a target value of 3000 ions. The raw files were reviewed with the SEQUEST engine against a database from the Uniprot protein sequence database. Parameters were set as follows: protein modifications included carbamidomethylation (C) (fixed), oxidation (M) (variable) and phosphorylation (S, T, Y) (variable); enzyme specificity was set to trypsin; maximal missed cleavages were set to two; the precursor ion mass tolerance was set to 10 ppm, and MS/MS tolerance was 0.5 Da.

2.13 | Murine neutrophil isolation

Murine neutrophils isolation was performed as previously described (Li et al., 2019). In brief, murine femur was perfused with 10 ml pre-chilled PBS and then the perfusate was centrifuged. The bone marrow cells were resuspended in 2 ml PBS. The suspension was then centrifuged over a Percoll gradient (72%, 60%, 52%) at 1100 × g for 30 min at room temperature. Neutrophils were collected in the band between the 72% and 60% layers.

2.14 | Biotinylated lung EV DNA pull-down

Biotinylated lung EV DNA pull-down was performed as previously described by Yang et al. (Yang et al., 2020). Biotinylated lung EV DNA was obtained using a biotin 3′ end DNA labelling kit (Beyotime). HEK293T cells were transfected with plasmids expressing Flag-tagged proteins and 24 h later, cells were lysed with Co-IP lysis buffer containing 150 mM NaCl, 1 mM EDTA, 20 mM Tris-HCl (pH 8.0), 10% glycerol, 0.5% NP-40 and protease inhibitor cocktail (Bimake). Cell lysates were then incubated with 300 ng biotinylated lung EV DNA for at least 4 h, before adding streptavidin-microbeads (GE HealthCare). After a 4 h incubation, the beads were washed with PBS-N (PBS containing 0.1% NP-40) four times and eluted with SDS–PAGE loading buffer, followed by immunoblot analysis.

2.15 | In vivo treatment

Each mouse was typically treated with lung EVs containing 50–100 ng DNA (before DNase I treatment if needed). This dose was usually 25%–50% of all lung EVs extracted from one mouse. Lung EVs were diluted in an appropriate volume of PBS based on the mode of administration (250 μl for intraperitoneal injections, 100 μl for intravenous injections, 20 μl for intranasal instillations). To test for dose-dependence, lung EVs containing 20 ng, 50 ng and 100 ng DNA were administered to mice. In addition, the non-vesicular components used as a control contained the same amount of DNA. In the thioglycolate-induced peritonitis model or the *Salmonella* Typhimurium-induced infection model, lung EVs (regardless of DNase I treatment or not) or non-vesicular components were administered to mice by intraperitoneal injection three days prior to the establishment of models.

In the GW4869-mediated lung EV inhibition experiments, the GW4869 (MCE, 1.25 mg/kg) was given nasally for 2 consecutive days prior to the establishment of models.

2.16 | In vitro treatment

Murine neutrophils derived from bone marrow or human leukocytes isolated from peripheral blood were all cultured in 24-well plates (8×10^5 per well) in RPMI-1640 medium (10% FBS, 1% penicillin/streptomycin). Cells in each well were typically treated with lung EVs containing 50 ng DNA (before DNase I treatment if needed) for 18 h. To test for dose-dependence, lung EVs containing 20 ng, 50 ng and 100 ng DNA were added. Depending on the experiment, pre-treatment of TLR9 inhibitor (1 μg/ml for ODN2088 (Tsingke Biological Technology) or 0.25 μM for E6446 (Psaitong)) for 5 h, or NF-κB inhibitor (50 μM, Beyotime) for 2 h was performed before incubation with lung EVs. Culture supernatants were collected for chemokine analysis and cells were lysed and RNA extracted for qPCR analysis.

2.17 | Thioglycolate-induced peritonitis model

Mice were intraperitoneally injected with 1 ml sterilized 3% (w/v) thioglycolate (Sigma-Aldrich). Peritoneal cells and peripheral blood cells were harvested after 3 h and analysed by flow cytometry (BD LSRFortessa).

2.18 | LPS-induced inflammation model

Mice were intraperitoneally injected with LPS at 10 mg/kg body weight (O55: B5, Sigma-Aldrich). Lung EVs were isolated 12 h post challenge followed by quantitative analysis.

2.19 | *Salmonella* Typhimurium-induced infection model

Salmonella Typhimurium (ATCC) was grown aerobically at 37°C in Luria–Bertani (LB) medium (10 g/L tryptone, 5 g/L yeast extract and 5 g/L NaCl). CFUs (colony-forming units) were measured through optical density with wavelength of 600 nm (OD600). Before infection, *S.* Typhimurium was harvested at log-phase (OD600 = 0.6 ∼ 0.8), washed with PBS, and then resuspended in PBS to a concentration of 2×10^7 CFU/ml. Each mouse was then inoculated intraperitoneally with 0.5 ml bacterial suspension (1×10^7 CFU). Neutrophils in peritoneal fluid and peripheral blood were detected by flow cytometry 3 h after infection. For survival analysis, infected mice were monitored hourly, and moribund animals were sacrificed by CO_2 asphyxiation. For analysis of bacterial burden in the liver and spleen, infected mice were sacrificed 12 h post infection. Next, the liver and spleen

were weighed, homogenized in pre-chilled PBS, diluted, and plated on LB plates for CFU measurement. For analysis of the bacterial load in the circulatory system, equal amount of anticoagulated peripheral blood ($\sim$200 μl) was collected from each mouse 12 h post infection and followed by bacterial DNA extraction (Magen). The absolute DNA content of gene STM4200 (primer sequences listed in Supplementary Table 4), which encodes a putative phage tail fibre protein of *S*. Typhimurium, was assayed by qPCR with a standard curve.

2.20 | Flow cytometry

For flow cytometric analysis, cells were pre-incubated with purified anti-CD16/32 antibody (Thermo Fisher; clone: 93) to block Fc receptors. Neutrophils were stained with anti-mouse Ly6G-APC (Thermo Fisher; clone: RB6-8C5), anti-mouse CD11b-PE (Thermo Fisher; clone: M1/70), anti-mouse CD45-FITC (Thermo Fisher; clone: 30-F11) and anti-mouse Ly6C-BV421 (Biolegend; clone: HK1.4) for 30 min at room temperature, followed by analysed on a BD LSRFortessa.

The flow cytometric analysis of lung EVs stained with DiI, DAPI or SYTOX was also performed using the BD LSRFortessa, and calibration beads (50 nm, 100 nm, 200 nm, 300 nm and 500 nm; Beckman Coulter) were used as reference controls.

2.21 | Real-time PCR

Total RNA was obtained from cells or tissues using a RaPure Total RNA Micro kit (Magen) and reverse transcribed with a 5 × All-in-one RT Master Mix (ABM). The reverse-transcription product was amplified with a Taq Pro Universal SYBR qPCR Master Mix (Vazyme) and analysed with gene-specific primers on an ABI 7500 system (Thermo Fisher). The sequences of the qPCR primers used are listed in Supplementary Table 4.

2.22 | Immunoblotting analysis

Total proteins were extracted using RIPA lysis buffer (50 mM Tris-HCl (pH 7.4), 150 mM NaCl, 1% NP-40, 1% sodium deoxycholate and 0.1% SDS) containing protease inhibitors. Protein concentrations of the supernatants were measured using a BCA assay kit (Thermo Fisher). Proteins were resolved by SDS–polyacrylamide gel electrophoresis and immunoblotted using antibodies against the following proteins: GM130 (Abcam), Calnexin (Abclonal), TOM20 (Abclonal), VDAC1 (Abclonal), ALIX (Abcam), CD9 (Abcam), CD81 (Proteintech), AGER (Affinity), GPRC5A (Affinity), TSG101 (BD Bioscience), Flotillin1 (BD Bioscience), Flag (Sigma Aldrich) and β-actin (ZSGB-Bio).

2.23 | DNA extraction and analysis

DNA was extracted from the sucrose fractions of the EV samples using an Animal tissue Genomic DNA Kit (Zomanbio) according to the manufacturer's instructions. Samples were treated with Proteinase K solution (Solarbio) and RNase A (TIANGEN) before DNA extraction. DNA concentrations were analysed using a Qubit 3.0 fluorometer with Qubit dsDNA HS and dsDNA BR kits (Thermo Fisher).

2.24 | Whole-genome-sequencing and bioinformatic analysis of lung EV DNA

Genome DNA from mouse pulmonary cells (P300g) and lung EV DNA were extracted. And the clustering of the index-coded samples was performed on a cBot Cluster Generation System using Novaseq 6000 S4 Reagent Kit (Illumina). After cluster generation, the DNA libraries were sequenced on Illumina NovaSeq 6000 platform. The sequencing reads were paired-end 150 bp.

The FASTQ files were first quality-controlled using Fast QC (version 0.11.9) and adapters were trimmed using Trimmomatic (version 0.39) (Bolger et al., 2014). The trimmed FASTQ files were then mapped to GRCh38 using Burrows-Wheeler Alignment tool (BWA, version 0.7.17) (Li & Durbin, 2009) and marked duplicates using GATK (version 4.2.0.0) and sorted, and indexed using Samtools (version 1.11) (Danecek et al., 2021). Cell samples were sequenced to an average depth of 23×, and EV DNA was sequenced to an average depth of 10×. Copy number alterations were called using cnvkit-0.9.9 (Talevich et al., 2016). The batch WGS method was used after calculating the sequence-accessible coordinates from the reference genome. CNVs were then called using the following command: cnvkit.py batch – method wgs sorted.bam -n -f path_to_genome/mm39.fa – output-reference flat_reference.cnn -d cnv/ -p 12 –scatter –diagram –annotate path_to_refFlat/refFlat.txt. Figures were generated using circos-0.69-9.

2.25 | Chemokine analyses

For chemokine analyses, multi-analyte profiling was performed using a ProcartaPlex Multiplex Immunoassay System (Thermo Fisher) according to the manufacturer's instructions. The panel measured protein levels of CXCL1 (GRO-α), CXCL2 (MIP-2), CXCL10 (IP-10), CCL2 (MCP-1), CCL3 (MIP-1α), CCL4 (MIP-1β), CCL5 (RANTES), CCL7 (MCP-3), and CCL11 (Eotaxin).

2.26 | Bulk mRNA-seq library preparation

Murine neutrophils incubated under various conditions in vitro were lysed and total RNA extracted using a RaPure Total RNA Micro kit (Magen). A mRNA-seq library was generated using a VAHTS® mRNA-seq V2 Library Prep Kit for Illumina (Vazyme) according to the manufacturer's instructions. The libraries were sequenced with a Novaseq 6000 (Illumina).

2.27 | Pearson correlation analysis

Pearson correlation analysis of the expression of proteins in human lung cell samples with that of human lung EV samples based on the result of LC–MS/MS was conducted using the "cor" function in R package "gplots" and illustrated using R package "pheatmap".

2.28 | Identification of differentially expressed proteins between lung cell samples and lung EV samples

R package "limma" was used to screen for differentially expressed proteins between six human lung cell samples and six human lung EV samples. Benjamin & Hochberg false discovery rate (FDR) method was used as a P value adjustment. Adjusted $P < 0.005$ and log (fold change) $> = 1$ was considered statistically significant. The top 30 higher expressed proteins of human lung EV samples compared with human cell samples were illustrated using R package "pheatmap".

2.29 | Gene ontology (GO) analysis

GO analyses were performed using DAVID (https://david.ncifcrf.gov/) (Huang da et al., 2009).

2.30 | Combined analysis of scRNA-seq data of lung cells and LC–MS/MS data of lung EVs

We downloaded scRNA-seq data from Gene Expression Omnibus (GEO) (http://www.ncbi.nlm.nih.gov/geo). GSE133747 provided scRNA-seq data of lung cells from human and mouse.

The scRNA-seq analyses of the female mouse lung sample and all human lung samples from GSE133747 were performed using the "Seurat" package (v 3.0) implemented in R. Variable genes were determined for each sample using the "FindVariableFeatures" function. The "FindIntegrationAnchors" function was used to identify anchors between human lung samples and the "IntegrateData" function was used to integrate them together. All the scRNA-seq data were then clustered by the standard "Seurat" clustering pipeline. The "FindClusters" and "RunTSNE" functions were used to identify the cell clusters and visualize them.

The lists of human and mouse lung EV proteins from the LC–MS/MS data were specified by the following selection criteria: (1) the protein was simultaneously detectable in all samples (six samples for human and three samples for mouse); (2) the average peak area of the protein was greater than a certain value (2×10^5 for human samples and 1.5×10^7 for mouse samples). Finally, 583 human proteins and 589 mouse proteins were selected for subsequent analyses.

The "Cluster Markers," which are relatively more highly expressed within a given cluster than other clusters, were selected with a threshold of log (fold change) > 0.25 and P-adj < 0.05 using the "FindAllMarkers" function in the "Seurat" package. Then the list of "Cluster Markers" of each cluster and the list of lung EV proteins were overlapped. Thus, the human and mouse lung EV proteins were identified as "Cluster Markers", "Non-Cluster Markers" or "Not detected" (Supplementary Tables 1 and 2).

The expression levels of the 583 and 589 genes which encode the selected human and mouse lung EV proteins among the different lung clusters were then illustrated by the "DoHeatmap" function in the "Seurat" package.

In order to evaluate the ability of single cell or single cluster of cells to secrete EVs, we used the following method to calculate. The "Cell%" mentioned in the "Result" section represents the percentage of the cells of a chosen cluster in total cells.

The expression index of $Protein_i$ in $Cell_j$ ($Protein_{ij}$%) and the ability of EV secretion of $Cell_j$ (s-EV_j%) were calculated using the formulas below.

$$Protein_{ij}\% = \frac{Area_i}{\sum Area} \times \frac{Exp_{ij}}{\sum Exp_i} \times 100\%$$

$$s\text{-}EV_j\% = \sum Protein_{ij}\%$$

The ability of EV secretion of each cluster (t-EV%) could thus be attained by adding the s-EV% of each single cell in the same cluster together.

$$t\text{-}EV\%(ClusterA) = \sum_{cell_j \in ClusterA} s\text{-}EV_j\%$$

In these formulas, $Area_i$ represents the average peak area of $Protein_i$ in the result of LC–MS/MS of lung EVs, Exp_{ij} represents the expression level of gene that encodes $Protein_i$ in $Cell_j$ in the scRNA-seq data of lung cells.

2.31 | Gene set enrichment analysis (GSEA)

We applied the GSEA software (https://www.gsea-msigdb.org/gsea/index.jsp) (Subramanian et al., 2005, Mootha et al., 2003) for GSEA in four groups (i.e. immune cells vs. non-immune cells in human lung scRNA-seq data, immune cells vs. non-immune cells in mouse lung scRNA-seq data, ATII cells and B cells in human lung scRNA-seq data, ATII cells and T cells in mouse lung scRNA-seq data) focusing on gene set of EV release. The threshold of statistically significantly gene set was set to a nominal P-value < 0.05 with FDR adjusted P-value < 0.25. In human lung clusters, monocytes, T cells, macrophages, NK cells, DCs, B cells and mast cells were designated as immune cells, whereas other types of cells were designated as non-immune cells. In mouse lung clusters, B cells, T cells, macrophages, monocytes, NK cells, neutrophils and DCs were designated as immune cells, whereas other types of cells were designated as non-immune cells. Based on previously published literature, 31 genes in the gene set of EV release are RAB5A, RAB5B, RAB27A, RAB27B, RAB11A, RAB11B, RAB35, RAB15, RAB17, RAB26, STX7, STX5A, SYT7, SYT15, SYT16, SYTL1, SNAP23, YKT6, PDCD6IP, TSG101, HGS, VPS4A, VPS33A, VPS45, VPS28, VPS37A, CHMP6, CHMP3, CHMP2A, SDCBP, ARF66 (Yang et al., 2019).

We performed GSEA between the experimental group of neutrophils treated with lung EVs and the control group of neutrophils treated with PBS. The threshold of statistically significantly gene set was set to a nominal P-value < 0.05 with FDR adjusted P-value < 0.25. Ontology gene sets (Version 7.4, http://www.gsea-msigdb.org/gsea/downloads.jsp) were applied in the GESA analysis.

2.32 | Statistical analysis

Statistical analyses were performed using GraphPad Prism 7 and RStudio software (version 1.2.5042; RStudio Inc). All data are presented as means ± SEM. To assess differences between two groups, a two-tailed unpaired Student's t test was used. To compare intergroup differences, a two-way repeated-measures ANOVA followed by the Bonferroni post-test was used. Differences were considered significant when $*P < 0.05$, $**P < 0.01$, $***P < 0.001$, $****P < 0.0001$.

3 | RESULTS

3.1 | Isolation and characterization of lung EVs

We observed various EVs as well as MVEs in normal lung tissues using transmission electron microscopy (TEM) (Figure 1a). To collect high quality EVs from normal lung tissues, we developed and optimized a differential centrifugation-based protocol as shown in Figure 1b. To avoid cell disruption, we introduced a gentle digestion method without homogenization, filtration or shear stress (Supplementary Figure 1a). Viable cells after digestion accounted for 96.2% and 94.2% of the total cells in human
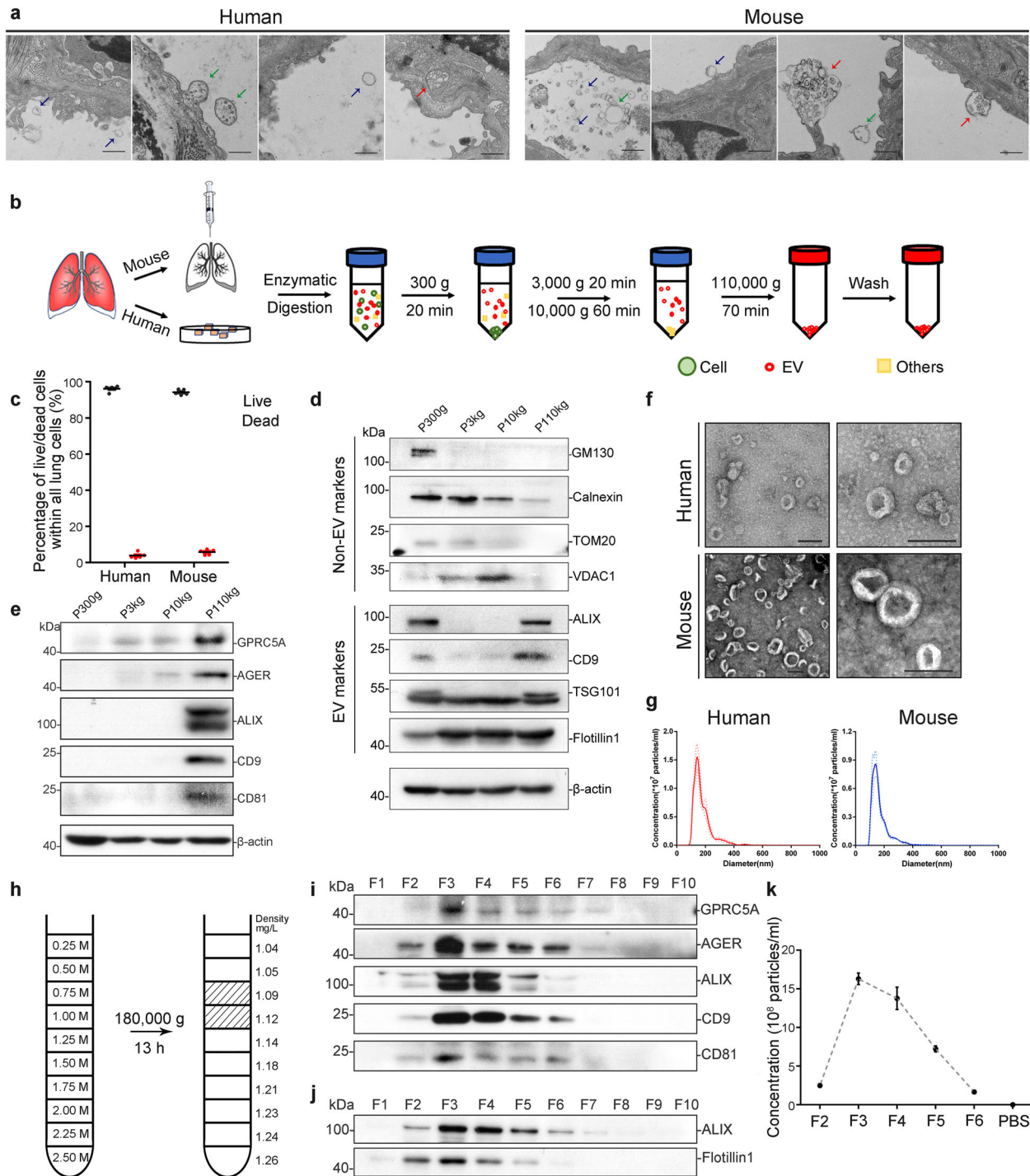
FIGURE 1 High-quality EVs are collected from human and murine lung tissues. (a) Representative TEM images of multiple extracellular vesicles and MVEs. Blue, green and red arrows indicated small EVs, large EVs and MVEs, respectively. Scale bars, 500 nm. (b) Schematic of EVs isolation from fresh human and murine lung tissues. (c) Percentage values of live and dead cells after digestion of human and murine lung tissues detected by flow cytometry (mean ± SEM; human samples $n = 4$, murine samples $n = 5$). (d) Immunoblotting analysis of protein extracts of the pellets from serial centrifugations of murine samples (P300 g, P3 kg, P10 kg, P110 indicated pellets of $300 \times g$, $3000 \times g$, $10,000 \times g$ and $110,000 \times g$ centrifugations, respectively). Immunoblotting was carried out using antibodies to GM130, Calnexin, TOM20, VDAC1, ALIX, CD9, TSG101, Flotillin-1, β-actin. (e) Immunoblotting analysis of protein extracts of the pellets from serial centrifugations of human samples. Immunoblotting was carried out using antibodies to GPRC5A, AGER, ALIX, CD9, CD81, β-actin. (f) Representative TEM images of lung EVs. Scale bars, 200 nm. (g) Size distribution of lung EVs detected by NTA (mean ± SEM; $n = 3$ acquisitions/sample). (h) Schematic of EV purification by sucrose density centrifugation. Densities of ten fractions are shown on the far right. Shaded fractions represent enrichment of lung EVs. (i) Immunoblotting analysis of protein extracts of the ten fractions of human lung EVs. Immunoblotting was carried out using antibodies to GPRC5A, AGER, ALIX, CD9, CD81. (j) Immunoblotting analysis of protein extracts of the ten fractions of murine lung EVs. Immunoblotting was carried out using antibodies to ALIX, Flotillin-1. (k) Numbers of particles in different fractions detected by NTA (mean ± SEM; $n = 3$ acquisitions/sample)
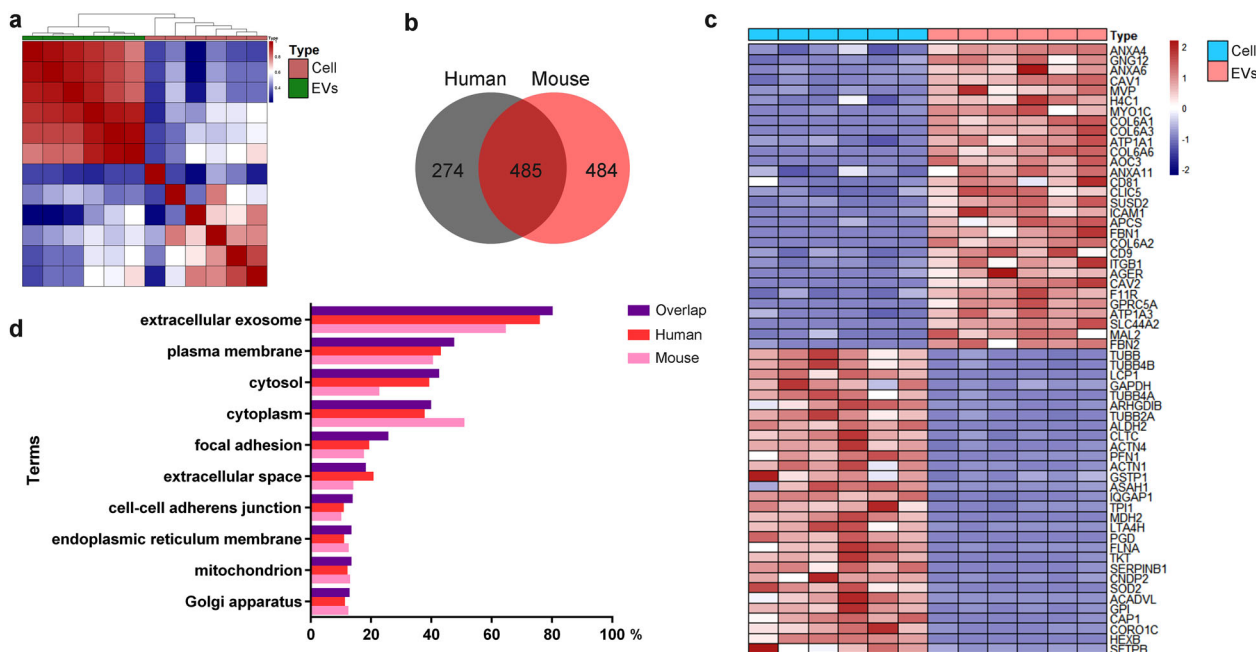
FIGURE 2 Protein profiling proves vesicle- and tissue-specificity of lung EVs. (a) Pearson correlation analysis of the expression of proteins between lung cells and lung EVs from human samples. (b) A Venn diagram of the proteins overlapping between human and murine lung EVs. (c) Differential expressed proteins between lung cells and lung EVs were identified using R package "limma." Adjusted $P < 0.005$ and log (fold change) ≥ 1 was considered as statistically significant. The top 30 higher expressed proteins in individual groups were illustrated by R package "pheatmap." (d) Analysis of EV proteins in human, mouse and overlapping sets using GO terms related to cellular component. The graph shows the percentage of proteins identified by mass spectrometry that fall into the designated GO category relative to the total number of proteins in the category. Top 10 categories in overlapping sets are shown

and murine samples, respectively (Figure 1c). This indicated that the lung cells were well protected during digestion, which was anticipated to substantially reduce the contamination of EV preparations by intracellular vesicles.

Following digestion, the mixed suspension was subjected to differential centrifugation to remove cellular debris and microvesicles. The pellets from different velocity centrifugations were analysed by immunoblotting. The results indicated that in murine samples, EV-associated proteins (ALIX, TSG101, CD9, CD81) were highly enriched in the 110,000 × g pellet (P110kg), while Golgi (GM130), endoplasmic reticulum (Calnexin) and mitochondrial proteins (TOM20, VDAC1) were undetectable or only weakly present in the P110kg fraction (Figure 1d). Similar enrichment of EV marker proteins in the P110kg fraction of human samples is shown in Figure 1e. TEM, nanoparticle tracking analysis (NTA) and cryo-electron tomography revealed similar morphology and size distribution of vesicles in the P110kg fraction from both the human and murine tissues (Figure 1f,g, Supplementary Figure 1b) consistent with the known characteristics of EVs (Lötvall et al., 2014).

To improve EV purity, samples were subjected to sucrose density centrifugation using a discontinuous ten-layer cushion of sucrose at concentrations ranging from 0.25 M to 2.5 M for 13 h of centrifugation at 180,000 × g (Figure 1h). Immunoblotting analysis of EVs after this prolonged, high-speed centrifugation revealed high enrichment of classical EV proteins in the third and fourth sucrose fractions (Figure 1i,j). NTA yielded similar results in that the third and fourth fractions had more particles than the other fractions (Figure 1k). The consistency of the Immunoblotting and NTA results indicated that the density of the lung EVs from both human and murine samples ranged from 1.05 to 1.14 g/ml. The average yield of EVs from lung tissue was 0.78 μg/mg for human samples and 0.70 μg/mg for murine samples (Supplementary Figure 1c).

Together, these results establish that high quality EVs which display the physical and biochemical properties and features of bona fide EVs can be efficiently collected from human and murine lung tissues by our modified isolation method.

3.2 | Proteomic analysis of lung EVs in human and mouse

Proteins contained in EVs are involved in specific cellular functions under various physiologic and pathologic conditions (Hoshino et al., 2020). To determine the protein components of lung EVs, we analysed EVs isolated from six human and three murine lung samples by liquid chromatography–tandem mass spectrometry (LC–MS/MS). To evaluate the overall correlation between proteomes derived from the different sources, we compared various sample types (i.e. lung cells vs. lung EVs) and species (i.e. human EVs vs. murine EVs) (Figure 2a–c). Lung EVs displayed a distinct protein profile compared with cells from lung tissues (Figure 2a). In addition to classic EV markers (CD9, CD81), lung specific EV markers (GPRC5A, AGER) were identified

(Figure 2c). Comparing with typical proteins in EVs, higher levels of proteins located at cytoskeleton (such as TUBB, ACTN1 and LCP1) and cytoplasm (such as ARHGDIB, CNDP2 and PGD) were detected in lung cells. Moreover, the proteomes of human and murine lung EVs were similar and more than half of the proteins detected were shared (Figure 2b).

We next performed a Gene Ontology (GO) enrichment analysis of the 759 human proteins, 969 murine proteins and 485 overlapping proteins identified by the LC–MS/MS analysis (Figure 2d). These studies showed that lung EV proteins, regardless of species, were highly enriched in the cellular component termed "extracellular exosome," "plasma membrane" and "cytosol," demonstrating the vesicular and extracellular nature of the proteins in the EVs. Importantly, enrichment analysis showed that EVs were not heavily contaminated with nuclear, Golgi, endoplasmic reticulum or blood microparticles, indicating that our modified isolation protocol enriched for EVs with minimal co-isolation of cellular debris or contaminating vesicles.

3.3 | Identification of GPRC5A and AGER as lung EV markers

Among the typical proteins that are more abundant in EVs than in cells (Figure 2c), GPRC5A and AGER which we determined were specifically expressed in lung tissue at the transcriptional level (Supplementary Figure 2a). Immunoblotting analysis also confirmed expression of these proteins in lung EV (Figure 1e,i, Supplementary Figure 2b). EGFP-tagged GPRC5A and AGER proteins were next used to observe their intracellular localization. Both proteins exhibited prominent assembly on the plasma membrane and intracellular vesicles (Supplementary Figure 2c). The fluorescence puncta corresponding to GPRC5A and AGER in the cytoplasm colocalized with the EV markers CD63 and CD9 (Supplementary Figure 2d). Thus, GPRC5A and AGER were identified as lung EV markers, which also corroborates the tissue source of the isolated EVs.

3.4 | ATII is the primary source of lung EVs

A variety of mammalian cells are able to release EVs, and the molecular composition of EVs can be a reflection of their original cell (Shao et al., 2018). ScRNA-seq is a powerful technique for dissecting the complexity of organs and tissues, helping us understand the basis of cell diversity and the heterogeneous transcriptional phenotypic states (Zhang et al., 2020). We attempted to identify the source of EVs by taking advantage of public scRNA-seq data and our LC–MS/MS results, following the process outlined in Figure 3a. Briefly, after obtaining scRNA-seq data of lung cells and proteomics data of lung EVs, we evaluated whether the protein composition of the lung EVs would reflect their cell of origin. Since more than half of the proteins in EVs were expressed in specific cell types, we calculated the proportion of EVs from each cell cluster based on their abundance (from LC–MS/MS data) and their expression levels (from scRNA-seq data). Finally, we calculated the ability of single cell to release EVs.

We used scRNA-seq data (GSE133747) from Gene Expression Omnibus (GEO) datasets. Following the procedures described (Lu et al., 2015), clustering in R package "Seurat" resolved 15 well-demarcated clusters from 17,370 human and 16 clusters from 3989 murine lung cells, including common immune cells and non-immune cells found in lung (Raredon et al., 2019) (Supplementary Figure 3a,b). We selected 583 high abundance EV proteins from the human (Supplementary Table 1) and 589 from the murine (Supplementary Table 2) LC–MS/MS results and generated heatmaps which showed that the genes encoding EV proteins had diverse expression levels among the different clusters (Supplementary Figure 3c,d). More than half of these genes could be identified as "Cluster Markers" by "Seurat" under the threshold of log (fold change) > 0.25, P-adj < 0.05 (Figure 3b). As shown in Figure 3b, "Cluster Markers" indicated proteins were specifically expressed in one or more clusters in scRNA-seq data. "Non-Cluster Markers" indicated that protein expressions showed no significant differences among clusters. "Not detected" indicated that proteins were not detected in the corresponding gene list of scRNA-seq. These results suggested that proteins in lung EVs could reflect their cell of origin, which was important for subsequent analyses (see Methods for details). Integrative analysis of the scRNA-seq and LC–MS/MS data indicated that ATIIs could account for most of the EVs, in both human and murine samples, indicating that ATIIs are the main source of EVs from lung tissue (Figure 3c,d).

Protein profiling was then used to evaluate the individual ability of single cells to release EVs. For human samples, we found that single fibroblasts released the most EVs (Figure 3e), whereas ATI cells released the most from murine samples (Figure 3f). In addition, we found that there were more EVs derived from single non-immune cells, compared to single immune cells (Figure 3g,h). Quantitative analysis of EVs in culture supernatants from a variety of human and murine cell lines showed similar results (Figure 3i). Using GSEA, we also identified a significant enrichment of EV secretion-related genes in all the non-immune cells compared with all the immune cells (Figure 3j). The up-regulated expression of EV secretion-related genes in non-immune cells is consistent with their greater ability to release EVs than immune cells.

Taken together, the above results demonstrate that our isolation and high-throughput detection methods have identified ATII cells as the main source of lung EVs and that non-immune cells generally release more EVs (per cell) than immune cells.
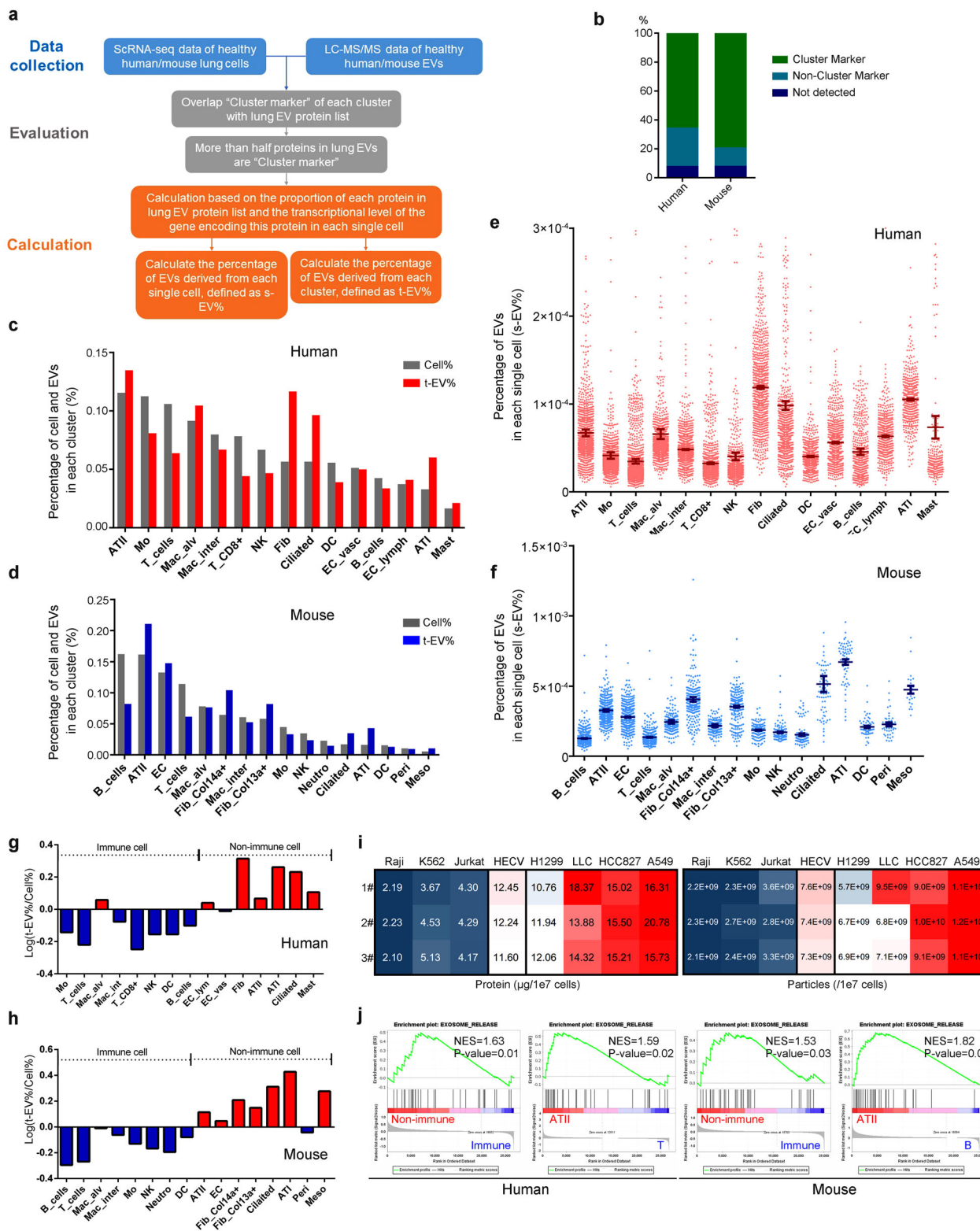
FIGURE 3 Analysis of EV proteomics together with scRNA-seq data assesses lung EV origin. (a) Schematic of the EV origin assessment by taking advantage of scRNA-seq data and LC–MS/MS results. (b) Percentage of lung EV proteins identified to be "Cluster Markers," "Non-Cluster Markers" or "Not detected" in human and mouse LC–MS/MS results. (c,d) Percentage of the number of cells of each cluster in total cells (Cell%) and percentage of EVs from each cluster (t-EV%) in human (c) and mouse (d) data, shown as classification of cell cluster. (e,f) Percentage of EVs from each single cell (s-EV%) in human (e) and mouse (f) data, shown as classification of cell cluster (mean ± SEM; n = cell number of each cluster). (g,h) Log(t-EV%/cell%) of each cell cluster in human (g) and mouse (h) data. (i) Quantification of particle and protein of EVs isolated from different cell lines including immune cell lines (human cell lines: Raji, K562, Jurkat) and non-immune cell lines (human cell lines: HECV, H1299, HCC827, A549; mouse cell line: LLC). (j) GSEA was performed focusing on gene set of EVs release in four groups, including immune cells and non-immune cells in both human and mouse lung scRNA-seq data, ATII and B in mouse scRNA-seq data, ATII and T in human scRNA-seq data
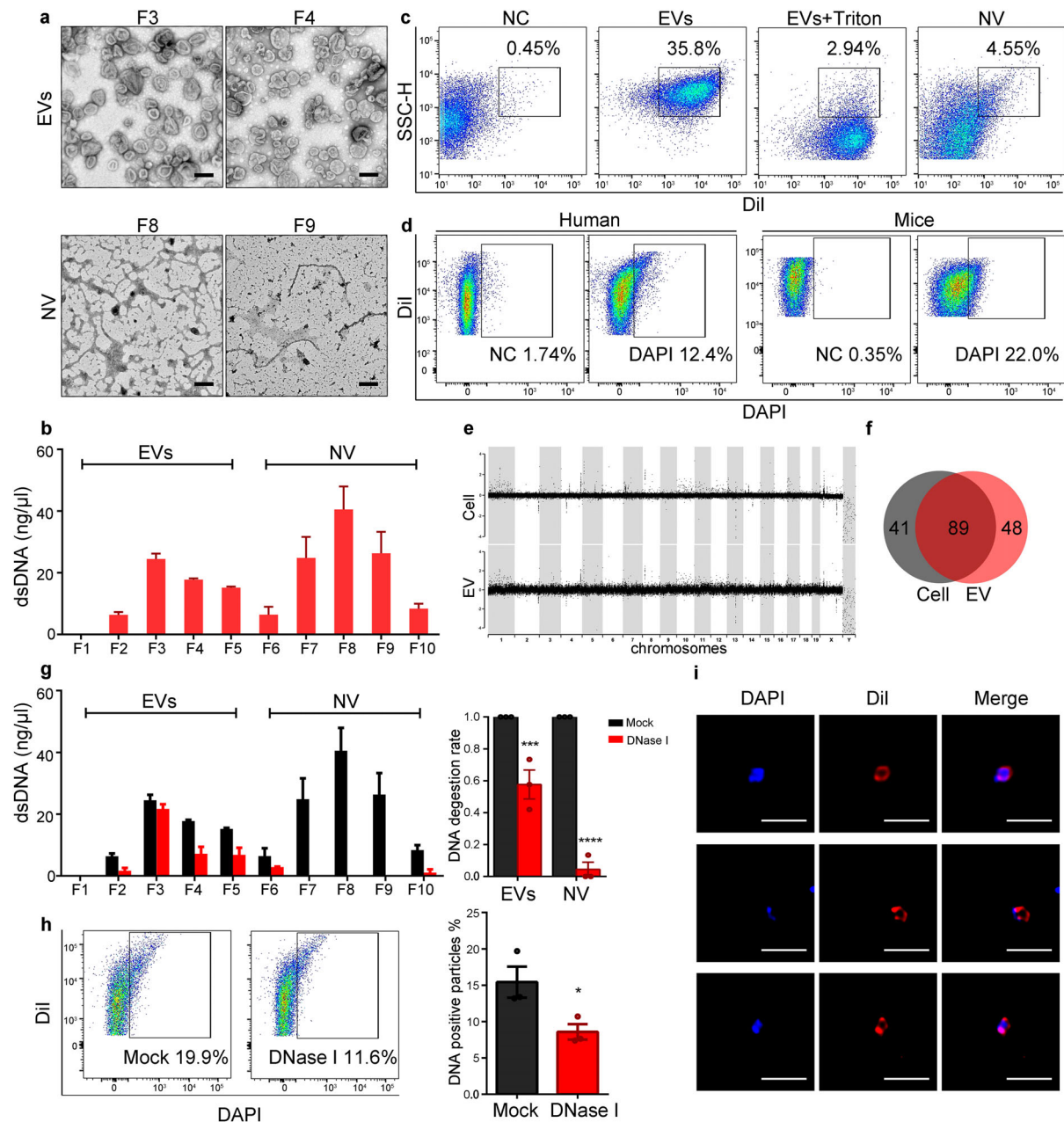
FIGURE 4 Lung EVs contain dsDNA. (a) Representative images of negative stain TEM of low-density fractions of lung EVs (F3, F4) and high-density fractions of non-vesicular components (F8, F9) after sucrose density centrifugation. NV, non-vesicular components. Scale bar: 200 nm. (b) Quantification of DNA extracted from ten fractions by Qubit (mean ± SEM, $n = 3$). NV, non-vesicular components. (c) Representative plots of lung EVs and non-vesicular components staining with DiI from flow cytometry analysis. NC, negative control. NV, non-vesicular components. (d) Representative plots of lung EVs staining with DAPI from flow cytometry analysis. (e) CNVs in chromosomes of both the EV-DNA and cellular DNA derived from murine lung tissue. (f) A Venn diagram of all the CNVs overlapping between the cellular and EV-DNA derived from murine lung tissues. (g) Quantification of DNA extracted from ten fractions treated with or without DNase I. Low-density fractions (F1–F5) were collected as EVs and high-density fractions (F6–F10) were collected as non-vesicular components. NV, non-vesicular components. (mean ± SEM, $n = 3$). (h) Flow cytometry analysis of DAPI positive lung EVs treated with DNase I or not (mean ± SEM, $n = 3$). Statistics by two-tailed unpaired Student's t test (*, $P < 0.05$). (i) Representative images of DAPI positive lung EVs labelled with DiI. Scale bars, 500 nm

3.5 | Lung EVs contain dsDNA

It has been reported that dsDNA and nuclear proteins are present in tumour derived EVs (Balaj et al., 2011). However, others have reported that dsDNA is associated with high density pools of non-vesicular components rather than purified EVs after gradient centrifugation (Jeppesen et al., 2019). Thus, it was of considerable interest to determine if dsDNA could be detected in our lung tissue derived EVs. Based on EV markers (Figure 1i,j) and observed morphology (Figure 4a), we identified low-density lung

EVs (1.05–1.14 g/ml) and high-density non-vesicular components (1.18–1.24 g/ml) in distinctly different fractions of our sucrose gradients, similar to that described by Jeppesen et al. (Jeppesen et al., 2019). However, after quantifying extracted dsDNA from the different fractions, it became apparent that dsDNA was distributed among the fractions in a bimodal fashion (Figure 4b). Treatment of extracted nucleic acids with DNase and RNase confirmed the isolation of pure DNA (Supplementary Figure 4a). These results demonstrate that dsDNA is present in both low-density lung EVs and high-density non-vesicular components.

To assess dsDNA-containing EVs at a single particle level, we used flow cytometry after staining lung EV membranes with DiI. A distinct cluster of red fluorescence positive particles was observed after staining which was absent after treatment with 0.5% Triton X-100 to disrupt lipid membranes (Figure 4c). Using a set of calibration beads, we assessed the diameter of the gated particles to be 100–200 nm (Supplementary Figure 4b), which was consistent with the results of the NTA (Figure 1g). Thus, we were able to identify lung EVs successfully by flow cytometry, whereas the non-vesicular components were not detected because they lack a membrane structure (Figure 4c). As shown in Figure 4d, approximately 10–20% of both human and murine lung EVs were positive for dsDNA after staining the EVs with DAPI. Next, we performed whole-genome sequencing of DNA from both intact lung cells (P300g) and lung EVs isolated from mice samples. The results showed that the lung EVs contained various lengths of dsDNA fragments which spanned all chromosomes, but no mitochondrial DNA was detected (Figure 4e). In addition, the copy number variations (CNVs) in the cellular and EV DNA were quite similar (Figure 4f). Together, these data indicate that the dsDNA in lung EVs originates from genomic DNA.

3.6 | DNA is present both inside and outside of lung EVs

To localize the DNA in lung EVs, they were treated with DNase I to degrade DNA attached to the outer membrane. This resulted in an approximately 40% reduction in total DNA (Figure 4g). Flow cytometry showed a similar reduction of DAPI positive particles after DNase I treatment (Figure 4h). On the other hand, little to no dsDNA was detected in non-vesicular components after DNase I treatment, consistent with a previous report (Jeppesen et al., 2019) (Figure 4g). We also used SYTOX Green nucleic acid stain, which does not cross intact membranes, to label DNA present outside or on the surface of EVs. The results showed that 40% of the lung EVs were SYTOX positive (Supplementary Figure 4c). Furthermore, we observed co-localization of DNA and the vesicular membrane structure by confocal microscopy after staining EVs with DAPI and DiI (Figure 4i). Collectively, these data strongly indicate that DNA is present both on the surface of and inside the lung EVs.

3.7 | Accumulation of lung EVs in bone marrow neutrophils

EVs deliver their cargo across cells and between organs, leading to alterations in the recipient cells (Tkach & Thery, 2016). To explore the biological functions of lung EVs, we first investigated where they accumulated. To assess the biodistribution of lung EVs in mice, DiR-labelled lung EVs were injected into C57BL/6 mice via the tail vein; DiR-labelled liposomes were used as a control. The animals were then examined using an in vivo imaging system (IVIS). We found that the lower limbs in mice injected with lung EVs showed high fluorescent signals compared to control mice injected with liposomes (Figure 5a). These results were corroborated by flow cytometry analysis, in which more red fluorescence was detected in the bone marrow of mice injected with DiI-labelled EVs relative to control mice (Figure 5b). We then examined the effect of different administration routes on lung EV distribution, namely tail intravenous injection, intraperitoneal injection and intranasal instillation. The results showed that different routes did not affect the accumulation of lung EVs at bone marrow and more cells with red fluorescence were detected in bone marrow through intravenous injection compared with the other two routes, indicating the lung EVs were transferred through blood vessels, as expected (Figure 5c). Using two-photon laser scanning microscopy for the intravital imaging of mouse lung tissues, we also observed red fluorescence labelled EVs in the intravascular space 24 h after an intranasal instillation of DiI-labelled EVs (Supplementary Figure 5a), supporting the conclusion that the lung EVs entered into the blood vessels. The red fluorescent cells in bone marrow were subsequently identified to be mainly neutrophils (52.7%) and monocytes (24.1%) (Figure 5d, Supplementary Figure 5b). Using confocal microscopy, we observed that lung EVs labelled with red fluorescence co-localized with neutrophils which were identified as CD45^{+} Ly6G^{+} cells (Figure 5e). Thus, our results suggest that transfer of lung EVs to bone marrow neutrophils occurs through blood vessels.

Another approach to examine the transfer of EVs in vivo is based on a system in which the EVs mediate the transfer functional Cre-mRNA into target cells. This system, which does not require any ex vivo manipulations, has been used successfully to visualize malignant cancer-derived EV transfer to benign cancer cells (Zomer et al., 2015). Thus, we adopted this system to explore whether lung EVs could transfer to bone marrow cells in vivo by using nasal instillation of adeno-associated virus (AAV) vectors AAV-Cre or AAV-GFP (control) into *ROSA26-CAG-LSL-tdTOMATO* mice (Figure 5f). We anticipated that lung EVs derived from Cre positive lung cells would transfer to recipient cells, resulting in TOMATO expression; no fluorescence would be detected in recipient cells in control group because GFP could not be transferred through EVs (Jiang et al., 2020). The results were consistent with this expectation. Thus, detection of red fluorescence in the bone marrow cells of mice receiving AAV-Cre
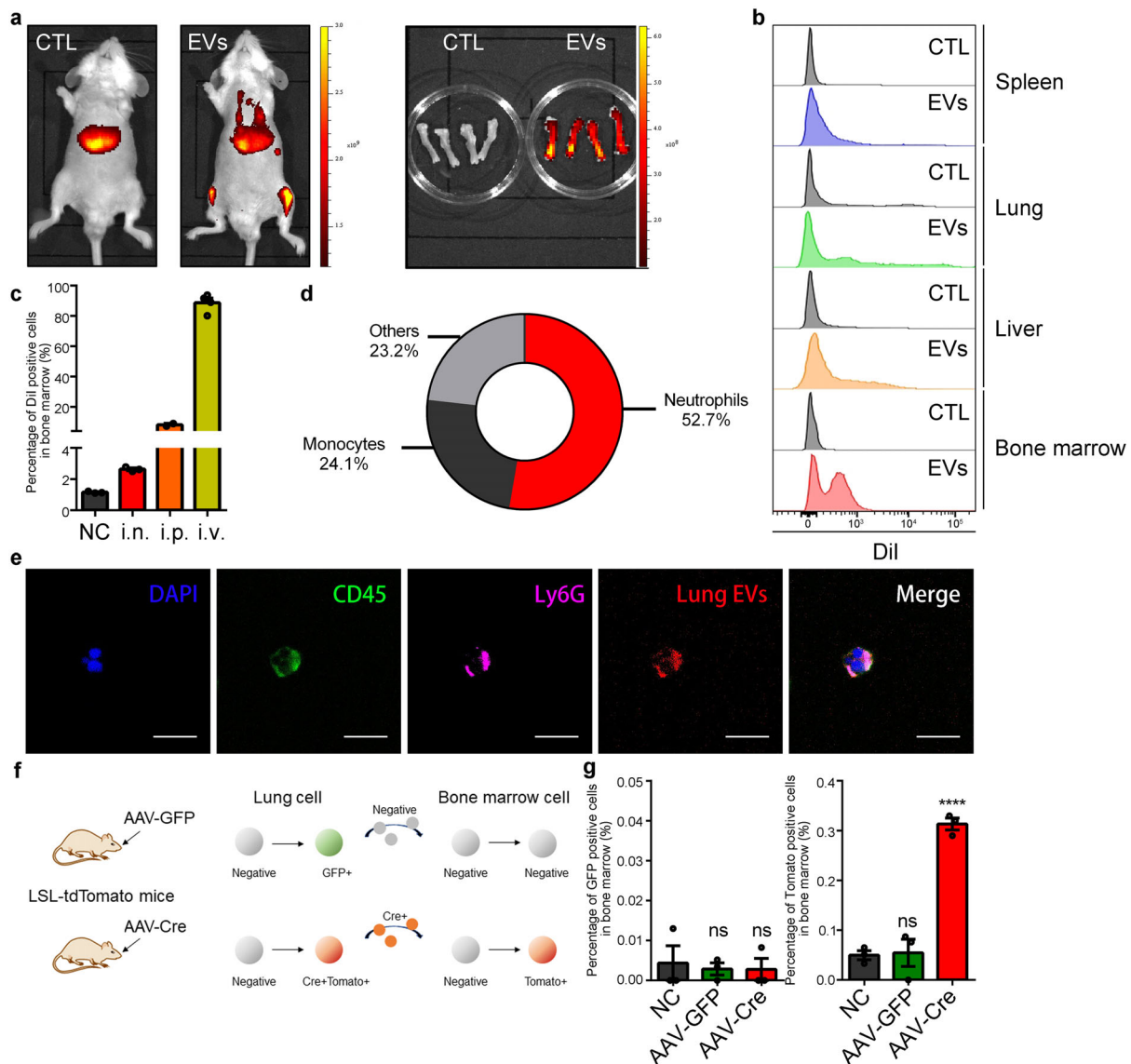
FIGURE 5 Lung EVs labelled with fluorescence are transferred into bone marrow. (a) Representative IVIS images of mice and their femurs 48 h post-injection with DiR-lung EVs or DiR-liposomes as control. (b) Representative images of DiI positive cells in different organs from mice 48 h post-injection with DiI-liposomes or DiI-lung EVs detected by flow cytometry. (c) Ratio of DiI positive cells in bone marrow detected by flow cytometry. Mice were injected with DiI labelled lung EVs in different routes 48 h before their bone marrow cells were harvested (mean ± SEM; $n = 3$). NC, negative control, without injection; i.n., intranasal instillation; i.p., intraperitoneal injection; i.v., tail intravenous injection. (d) Proportion of different cell types in DiI positive cells in bone marrow from mice injected with DiI labeled lung EVs. Neutrophils were gated with CD45$^+$ CD11b$^+$ Ly6G^{high} Ly6C^{low} and monocytes were gated with CD45$^+$ CD11b$^+$ Ly6G^{low} Ly6C^{high}. (e) Representative confocal image of DiI positive neutrophils isolated from mice injected with DiI labelled lung EVs. Scale bars, 20 μm. (f) System of *ROSA26-CAG-LSL-tdTOMATO* mice infected by AAV-GFP or AAV-Cre through nasal instillation. (g) Ratio of cells with GFP or Tomato in bone marrows from mice treated with AAV-GFP or AAV-Cre through nasal instillation for 4 weeks (mean ± SEM; $n = 3$). Statistics by two-tailed unpaired Student's t test (****, $P < 0.0001$. ns, not significant, $P > 0.05$)

verified EV-mediated transfer from lung cells to bone marrow cells in vivo, whereas green fluorescence was absent from the bone marrow cells of control group mice (Figure 5g, Supplementary Figure 5c,d). Collectively, these data provide convincing evidence that lung EVs can be transferred into blood vessels and ultimately accumulate in bone marrow neutrophils.

3.8 | Lung EV-DNA enhances chemotaxis of neutrophils

To further investigate the function of lung EVs in neutrophils, we first examined the relative proportions of various bone marrow cells following intraperitoneal injection of lung EVs. However, no significant differences were found between mice treated with lung EVs and mice treated with PBS as control (Supplementary Figure 6a,b). We next tested whether chemotaxis was affected

in neutrophils treated with lung EVs because this process of sensing and moving toward a chemoattractant is an important characteristic of circulating effector leukocytes including neutrophils (Li et al., 2019). Therefore, we employed a thioglycolate-induced model of acute peritonitis for this purpose (Li et al., 2019). We found that 3 h after administration of thioglycolate, mice injected 3 days previously with three different amounts of lung EVs showed a dose-dependent increase in the number of neutrophils recruited to the peritoneal lavage site compared to control mice receiving PBS alone (Figure 6a,b). In contrast, there were no differences in the number of neutrophils in the peripheral blood of PBS or EV treated mice (Figure 6c). These data indicate that the lung EVs promoted the migration of neutrophils rather than increasing their numbers in peripheral blood. GW4869, a neutral sphingomyelinase (nSMase) inhibitor, blocks EV secretion through the ESCRT (endosomal sorting complex required for transport) independent pathway (Trajkovic et al., 2008). After two doses of GW4869 via nasal instillation, the amount of DNA, protein and numbers of lung EVs were greatly decreased (Supplementary Figure 6c). These observations indicated that GW4869 successfully inhibited the release of endogenous lung EVs. We subsequently tested the migration of neutrophils after GW4869 treatment and found the number of neutrophils recruited into the abdominal cavity in GW4869-treated mice decreased significantly (Supplementary Figure 6d). These results support the conclusion that lung EV deficiency leads to an inhibition of neutrophil chemotaxis.

It has been reported that EV derived DNA can modulate tumour immunity via paracrine interactions and activation of cytosolic DNA sensor pathways (Diamond et al., 2018). Consequently, we speculated that lung EV-DNA is involved in regulating the chemotaxis of neutrophils. As shown in Figures 6d–f, incubation of lung EVs with DNase I before injecting them into mice reduced the ability of the lung EVs to promote neutrophil chemotaxis. Because DNase I treatment only reduced the quantity of DNA without affecting levels of protein, RNA, or reducing EV number or EV diameter (Figure 6g–i), this indicates that the lung EV-DNA was responsible for upregulation of chemotaxis. Furthermore, the non-vesicular component with same DNA content had no effect on neutrophils showing values comparable to those of control mice treated with PBS (Figure 6d–f). In addition, there were no differences in neutrophil levels in peritoneal lavage fluid and peripheral blood before thioglycolate induction among these groups (Supplementary Figure 6e,f), indicating EV injection did not influence neutrophil biodistribution in mice in a non-inflammatory condition. Together, these findings strongly support the conclusion that the DNA in lung EVs enhances neutrophil chemotaxis in vivo.

3.9 | Lung EV-DNA induces the expressions of CXCL1 and CXCL2 in neutrophils

To further study the effects of lung EVs on neutrophils, we carried out mRNA sequencing analysis of mouse neutrophils isolated from bone marrow and stimulated with mouse lung EVs in vitro. The results showed that the transcriptional levels of pro-inflammatory chemokines were markedly upregulated after lung EVs treatment (Figure 7a). In addition, using GSEA, we observed a significant enrichment of neutrophil chemotaxis-related genes in the lung EVs stimulated group compared with the control group (Figure 7b), further supporting the idea that lung EVs can promote neutrophil chemotaxis. We then performed a cytokine array on the supernatants of cultured neutrophils (Figure 7c). Compared to untreated neutrophils and neutrophils stimulated by lung EVs pretreated with DNase I, the lung EV-stimulated neutrophils displayed substantial increases in the secretion of various chemokines in a dose-dependent manner. Since CXCL1 and CXCL2 are known to contribute to the early stages of neutrophil mobilization and recruitment during acute inflammation (Burdon et al., 2005; Girbl et al., 2018), we next focused on characterizing the production of these chemokines by neutrophils. We found that lung EVs very efficiently stimulated neutrophils to produce CXCL1 and CXCL2, whereas incubation of lung EVs with DNase I before their co-culture with neutrophils reduced this effect (Figure 7d, Supplementary Figure 7a). We also observed a significant increase in CXCL1 and CXCL2 levels in neutrophils isolated from mice treated with lung EVs compared with control mice, while lung EVs pre-incubated with DNase I showed only a slight increase, confirming a change in the neutrophil transcriptional program in vivo (Figure 7e). In addition, we observed a significant decrease of CXCL1 and CXCL2 levels in neutrophils isolated from GW4869 treated mice compared with the control mice (Supplementary Figure 7b). Together, these results demonstrate that lung EV-DNA induce CXCL1 and CXCL2 release from bone marrow neutrophils both in vitro and in vivo.

We next investigated the effects of lung EVs in human samples. Leukocytes were isolated from human peripheral blood and co-cultured with lung EVs from human lung tissue. Once again, we found that human lung EVs substantially increased CXCL1 and CXCL2 expression levels in leukocytes whereas human lung EVs pretreated with DNase I did not (Supplementary Figure 7c,d). These results support the conclusion that lung EVs increase the expression of CXCL1 and CXCL2 in neutrophils both in humans and in mice.

3.10 | TLR9 senses lung EV-DNA in neutrophils

We next tested the molecular pathway by which lung EV-DNA induces chemotaxis of neutrophils. TLR9, localized in plasma membrane and endosomes, senses DNA with unmethylated CpG motifs derived from bacteria and viruses, resulting in activation
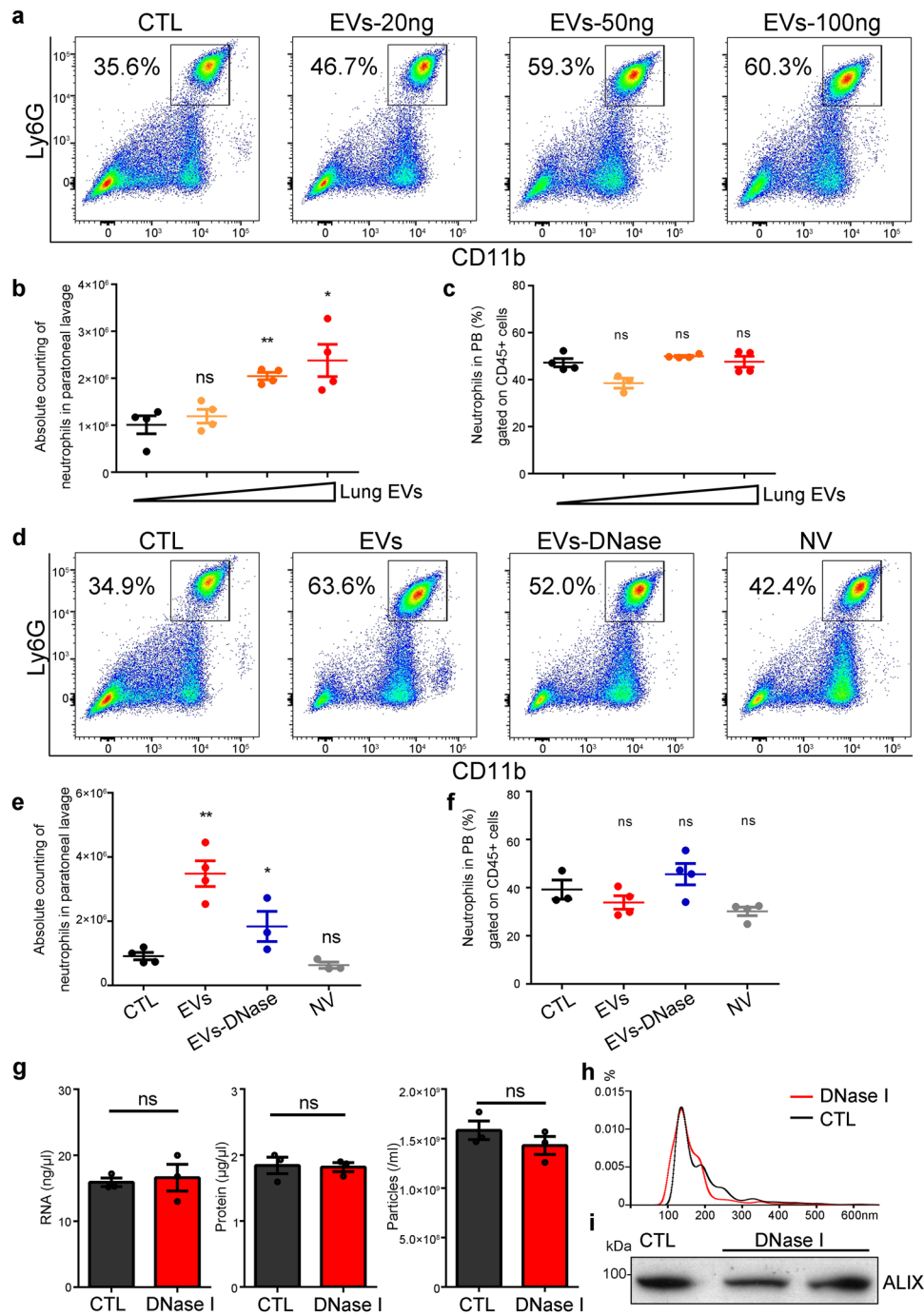
FIGURE 6 Lung EV-DNA enhances chemotaxis of neutrophils. (a) Representative flow cytometry plots for neutrophils recruited in peritoneal cavity 3 h after intraperitoneal injection with thioglycolate. Mice were injected with gradient doses of lung EVs or equal volume of PBS 3 days before in a–c. (b) Absolute number of neutrophils recruited in peritoneal cavity 3 h after intraperitoneal injection with thioglycolate (mean ± SEM; $n = 4$). Statistics by two-tailed unpaired Student's t test (*, $P < 0.05$. **, $P < 0.01$. ns, not significant, $P > 0.05$). (c) Proportion of neutrophils in CD45$^+$ cells in peripheral blood 3 h after intraperitoneal injection with thioglycolate (mean ± SEM; $n = 3$–4). Statistics by two-tailed unpaired Student's t test (ns, not significant, $P > 0.05$). (d) Representative flow cytometry plots for neutrophils recruited in peritoneal cavity 3 h after intraperitoneal injection with thioglycolate. Mice were injected with lung EVs, lung EVs pretreated with DNase I, non-vesicular components with equal DNA content or equal volume of PBS 3 days before in d–f. NV, non-vesicular components. (e) Absolute number of neutrophils recruited in peritoneal cavity 3 h after intraperitoneal injection with thioglycolate. (mean ± SEM; $n = 3$–4). Statistics by two-tailed unpaired Student's t test (*, $P < 0.05$. **, $P < 0.01$. ns, not significant, $P > 0.05$). (f) Proportion of neutrophils in CD45$^+$ cells in peripheral blood 3 h after intraperitoneal injection with thioglycolate (mean ± SEM; $n = 3$–4). Statistics by two-tailed unpaired Student's t test (ns, not significant, $P > 0.05$). (g) Quantification of protein, RNA and particle concentration of lung EVs treated with or without DNase I (mean ± SEM, $n = 3$). Statistics by two-tailed unpaired Student's t test (ns, not significant, $P > 0.05$). (h) Size distribution of lung EVs treated with or without DNase I detected by NTA (mean ± SEM; $n = 3$ acquisitions/sample). (i) Immunoblotting analysis of protein extracts of lung EVs treated with or without DNase I. Immunoblotting was carried out using antibodies to ALIX
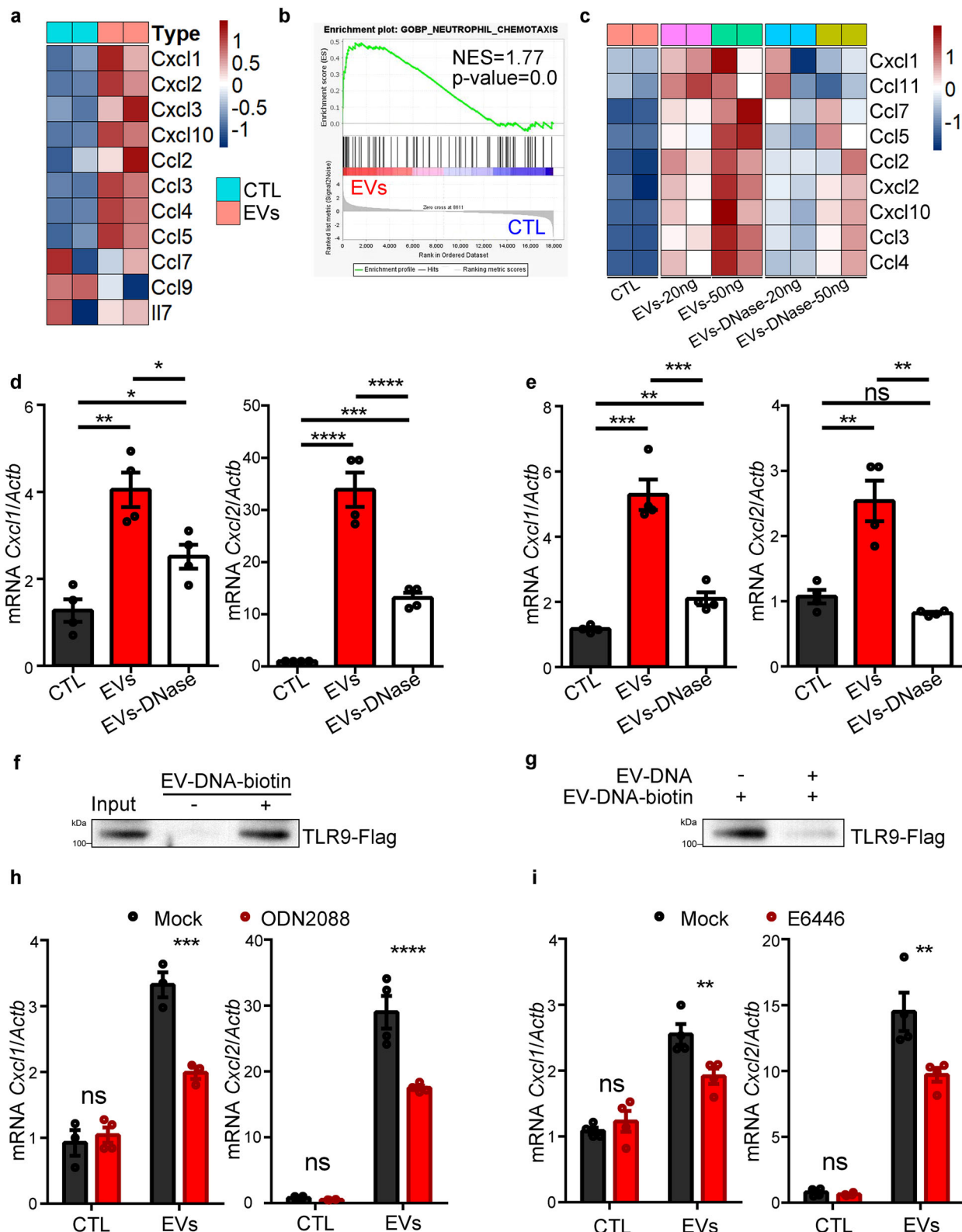
FIGURE 7 Lung EV-DNA triggers the release of neutrophil mobilizing chemokines through TLR9 signaling. (a) mRNA sequencing analysis of chemokine and cytokine levels in neutrophils treated with lung EVs or PBS as control for 18 h. (b) GSEA was performed focusing on neutrophil-chemotaxis genes between neutrophils treated with lung EVs and neutrophils treated with PBS as control. (c) Representative cytokine array panels of supernatants taken from 18 h culture of neutrophils incubated with lung EVs, lung EVs pretreated with DNase I, or PBS as control. (d) Real-time PCR analysis of *Cxcl1* and *Cxcl2* levels in murine neutrophils treated with lung EVs, lung EVs pretreated with DNase I or PBS as control for 18 h (mean ± SEM; $n = 4$). Statistics by two-tailed unpaired Student's t test (*, $P < 0.05$. **, $P < 0.01$. ***, $P < 0.001$. ****, $P < 0.0001$). (e) Real-time PCR analysis of *Cxcl1* and *Cxcl2* levels in neutrophils isolated from mice injected with lung EVs, lung EVs pretreated with DNase I or PBS as control (mean ± SEM; $n = 4$). Statistics by two-tailed unpaired Student's t test (**, $P < 0.01$. ***, $P < 0.001$. ns, not significant, $P > 0.05$). (f) Lysates of HEK293T transfected with Flag-tagged TLR9 were incubated in the presence or the

of NF-κB and downstream inflammatory pathways (Ahmad-Nejad et al., 2002; Hemmi et al., 2000; Latz et al., 2004; Leifer et al., 2004). It has been reported that neutrophils can be activated by mitochondrial DNA through TLR9 signalling and cause inflammatory responses to injury (Zhang et al., 2010). Thus, we investigated whether or not TLR9 sensed DNA in lung EVs. Accordingly, TLR9 binding to lung EV-DNA was assessed using an in vitro DNA-binding pull-down assay (Yang et al., 2020). The result showed that TLR9 was enriched from lysates of TLR9-overexpressing HEK293 cells by incubating biotinylated lung EV-DNA with streptavidin beads (Figure 7f). Furthermore, binding was efficiently competed by unbiotinylated lung EV-DNA (Figure 7g), suggesting TLR9 could bind to lung EV-DNA. In addition, we observed the colocalization of DiI-labelled lung EVs with endogenous TLR9 in neutrophils by confocal microscopy (Supplementary Figure 7e). These results indicate that TLR9 has the ability to sense lung EV-DNA.

TLR9 can be activated by the synthetic oligodeoxynucleotides ODN1668 that contains unmethylated CpG, but is inhibited by ligands such as ODN2088, in which "GCGTT" in ODN1668 is replaced with "GCGGG" (Stunz et al., 2002). Another inhibitor, E6446 {6-[3-(pyrrolidin-1-yl)propoxy)-2-(4-(3-(pyrrolidin-1-yl)propoxy)phenyl]benzo[d]oxazole}, is a synthetic antagonist of nucleic acid–sensing TLRs and specifically inhibits TLR9 activation in vitro (Lamphier et al., 2014). Using ODN2088 and E6446 to block the DNA-binding site of endogenous TLR9 in neutrophils, we tested whether lung EV-DNA was still able to stimulate neutrophils. Neutrophils incubated with lung EVs after treatment with ODN2088 (Figure 7h) or E6446 (Figure 7i) for 5 h effectively reduced CXCL1 and CXCL2 mRNA levels compared with neutrophils incubated with lung EVs only. Moreover, we found that inhibition of NF-κb by BAY11-7082 also abolished the effect of lung EVs (Supplementary Figure 7f). These results indicate that lung EV-DNA triggers the release of neutrophil mobilizing chemokines through TLR9 signalling.

Taken together, our findings indicate that DNA carried by lung EVs is sensed by TLR9 and directs transcriptional programs in bone marrow neutrophils, including pro-inflammatory chemokine production and release. These processes are critical for neutrophil mobilization from the bone marrow during the onset of acute inflammation. Moreover, our results show that inhibition of lung EV secretion or disruption of lung EV-DNA is sufficient to impair chemokine production by bone marrow neutrophils and to reduce their chemotactic response.

3.11 | Lung EVs enhance the recruitment of neutrophils in *Salmonella* infection

Neutrophils are a crucial component of the innate immune system and the initial defence of the body against extracellular pathogens. Notably, neutrophils are required to resist the onset or severity of sepsis from *Salmonella* infection (Li et al., 2019). The results reported above for the mouse models and our molecular findings led us to further assess the status of lung EVs in clinical infectious disease. Compared with non-infected mice, we detected higher levels of DNA in lung EVs isolated from mice injected with lipopolysaccharides (LPS) to mimic acute gram-negative bacterial inflammation or directly infected with gram-negative *Salmonella* Typhimurium by intraperitoneal injection (1×10^7 CFU/mouse), which suggested lung EVs participate in the process of bacterial infection (Figure 8a,b). Thus, we assessed neutrophil chemotaxis under *Salmonella* infection and found that mice pretreated with lung EVs showed a greater number of neutrophils recruited into the peritoneal lavage fluid than mice pretreated with PBS, lung EVs incubated with DNase I or non-vesicular components (Figure 8c,d). We also detected more neutrophils in peripheral blood as expected (Figure 8e,f), because the bacterial infection was systemic and thus differed from the thioglycolate induction model of peritonitis. Finally, we observed that mice pretreated with lung EVs survived significantly longer under acute infection compared with control mice (Figure 8g). Meanwhile, bacterial DNA in peripheral blood detected by real-time PCR (Figure 8h) and counts of viable CFU in liver and spleen tissues (Supplementary Figure 8a) were much lower in mice pretreated with lung EVs, which were coincident with the lifespan results. Moreover, we examined the impact of lung EV inhibition by GW4869 on bacterial infection and the results of survival time and bacterial DNA in peripheral blood showed that GW4869 treated mice had severer infection than DMSO treated mice (Figure 8i,j), which were further confirmed by the counts of viable CFU in spleen and liver tissues (Supplementary Figure 8b). Our findings indicated that lung EVs could effectively enhance neutrophils recruitment and inhibition of lung EVs secretion gives rise to a chemotaxis impairment in neutrophils that reduces host immune defence. These observations show that the regulatory mechanisms identified in the present work by which neutrophils respond to lung EV-DNA are also functional during bacterial infection with *Salmonella* Typhimurium and lung EV treatments prolong survival time of infected mice.

absence of biotinylated lung EV-DNA. The bound proteins were immunoprecipitated with streptavidin microbeads and blotted by an anti-Flag antibody. (g) Immunoblotting analysis for TLR9-Flag immunoprecipitated with biotinylated lung EV-DNA in the absence or in the presence of 1 μg unbiotinylated lung EV-DNA. (h–i) Real-time PCR analysis of *Cxcl1* and *Cxcl2* levels in bone marrow neutrophils pretreated with TLR9 inhibitory oligodeoxynucleotide ODN2088 (h) and inhibitor E6446 (i) for 5 h prior to incubation with or without lung EVs (mean ± SEM; $n = 4$). Statistics by two-way repeated-measures ANOVA followed by the Bonferroni post test (**, $P < 0.01$. ***, $P < 0.001$. ****, $P < 0.0001$. ns, not significant, $P > 0.05$)
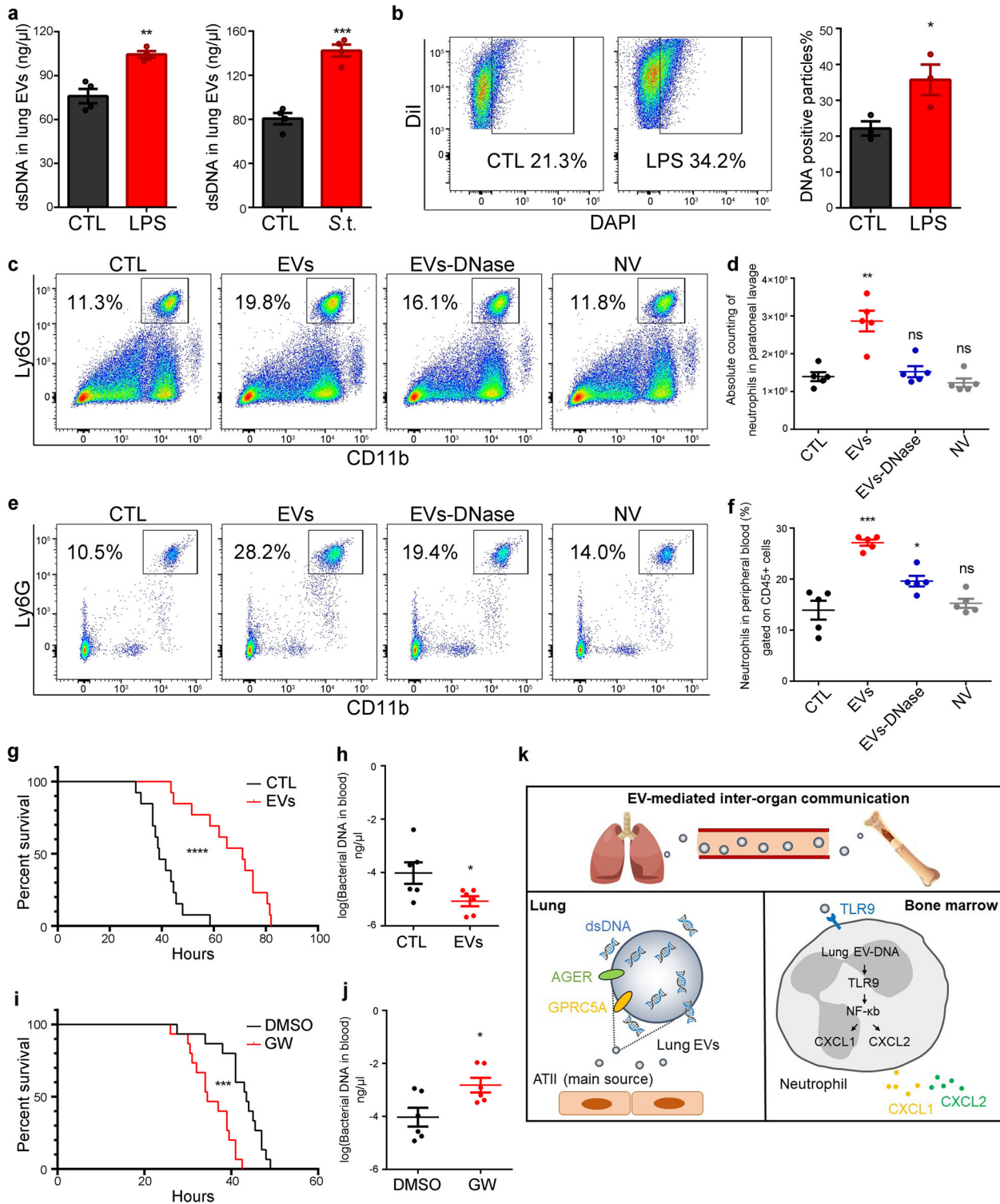
FIGURE 8 Lung EVs enhance the recruitment of neutrophils during *Salmonella* infection. (a) Quantification of dsDNA in lung EVs isolated from mice 12 h after injection with LPS ($n = 3$) or infection by *S. typhimurium* ($n = 4$). Statistics by two-tailed unpaired Student's *t* test (**, $P < 0.01$, ***, $P < 0.001$). (b) Flow cytometry analysis of DNA positive lung EVs (DAPI[+]) isolated from mice injected with PBS and LPS (mean ± SEM, $n = 3$). Statistics by two-tailed unpaired Student's *t* test (*, $P < 0.05$). (c) Representative flow cytometry plots for neutrophils recruited in peritoneal cavity 3 h post *S. typhimurium* infection. Mice were injected with lung EVs, lung EVs pretreated with DNase I, non-vesicular components with equal DNA content or equal volume of PBS 3 days before. NV, non-vesicular components. (d) Absolute number of neutrophils recruited in peritoneal cavity 3 h post *S. typhimurium* infection (mean ± SEM; $n = 5$). Statistics by two-tailed unpaired Student's *t* test (**, $P < 0.01$. ns, not significant, $P > 0.05$). (e) Representative flow cytometry plots for neutrophils in peripheral blood 3 h post *S. typhimurium* infection. (f) Proportion of neutrophils in CD45^{+} cells in peripheral blood 3 h post *S. typhimurium* infection (mean ± SEM; $n = 5$). Statistics by two-tailed unpaired Student's *t* test (*, $P < 0.05$. ***, $P < 0.001$. ns, not significant, $P > 0.05$). (g) Mouse survival curves post *S. typhimurium* infection. PBS treated mice and lung EV-treated mice were inoculated intraperitoneally with 1×10^7 CFU/mouse bacteria in g, h ($n = 13$). Statistics by

4 │ DISCUSSION

EVs isolated directly from tissues provide us with comprehensive biological information because the cells that they derived maintain the communication networks within the tissue microenvironment, and thus better approximate in vivoxg501 conditions than EVs isolated from cell culture supernatants (Crescitelli et al., 2021). Limited by the complexity of tissues and organs, effective methods of isolating EVs from tissues have been lacking until now. In this study, for the first time, we have established an effective method to enrich high quality EVs from lung tissue, with which we provide a molecular understanding of lung EVs and their regulatory role on bone marrow neutrophils (Figure 8e). We adopted a rigorous protocol that eliminates contamination by blood EVs and avoids cell disruption during tissue digestion, and thus better ensures the purity of the isolated EVs. Using immunoblotting, TEM, NTA and LC–MS/MS methods, we comprehensively analysed and characterized both human and murine lung EVs and found many similarities between the two species. In addition, we identified GPRC5A and AGER as protein markers of lung EVs, which will aid in determining the lung specificity of EVs. Furthermore, these proteins can potentially be employed in future to isolate lung EVs from plasma or other biofluids.

We have also developed a combination of high-throughput detection methods to evaluate the source of lung EVs and using these innovative methods, we determined that they are mainly derived from ATII cells. This result is consistent with previous studies, which reported that epithelial cells were the main source of EVs in the lung (Kulshreshtha et al., 2013, Bastarache et al., 2009). While Kulshreshtha et al. showed that EV marker proteins were mostly located in epithelial cells and alveolar macrophages in human lung tissue sections (Kulshreshtha et al., 2013), the ability of the expression and distribution of several classical protein markers to determine precisely the source of lung EVs is limited. Our methods take advantage of more than 500 highly expressed proteins in lung EVs and their expression levels in lung scRNA-seq data, thus providing a much more comprehensive and rigorous assessment. We also found that the ability of non-immune cells to release EVs was greater than that of immune cells. The difference in EV releasing ability among different cell types confirms that EVs are functional vesicles released from cells in a precisely controlled fashion.

We identified different characteristics between human and mice samples and speculated that it might be caused by the following reasons: (1) We removed blood to eliminate the plasma EVs in all experimental animals but not during treatment of human samples considering of the feasibility. Contamination of blood in tissues has impact on cell viability, EV recovery, and EV proteomic data (Li et al., 2021). (2) Deposits in human lung tissues, including air pollutants and particles, may cause differences in EV proteomic data comparing with murine lung EVs. (3) The healthy statuses of human and mice are inconsistent. Murine lung tissues were obtained from healthy mice, while human samples resected from patients undergoing a lobectomy for focal lung tumours and normal lung tissues were obtained from uninvolved regions greater than 5 cm from the edge of the tumours. (4) Technical variation, including batch effect (Hicks et al., 2018; Leek et al., 2010), cell-specific capture efficiency (Kolodziejczyk et al., 2015) and dropout (Haque et al., 2017; Sarkar & Stephens, 2021; Svensson et al., 2017) and biological variation, including stochastic gene expression (Hwang et al., 2018; Marinov et al., 2014) and cell cycle (Kolodziejczyk et al., 2015) affect the analysis of EV source. These factors potentially account for the species differences and allogenic differences, which needs further rigorous controlled experiments to clarify their effects.

In addition to proteins, we explored DNA in lung EVs. We identified dsDNA to be in both lung EVs and non-vesicle components. Specifically, various lengths of dsDNA fragments spanning all chromosomes are present both on the surface and inside of both human and mouse lung EVs. These findings indicate modes for active secretion of extracellular DNA in vivo are more diverse than previously assumed based on the results from cell-culture systems. Moreover, we provide evidence that lung EVs transfer to bone marrow neutrophils despite different administration routes and confirm the process in vivo by using Cre-loxp system, in which the EVs transfer functional Cre-mRNA into target cells without any ex vivo manipulations. Furthermore, we provide convincing evidence that dsDNA carried by lung EVs triggers the release of neutrophil mobilizing chemokines CXCL1 and CXCL2 through TLR9 signalling, suggesting physiological extracellular DNA exerts immune-regulatory functions through EV-mediated transportation. Notably, our findings show that lung EVs significantly promoted neutrophils recruitment into inflammatory sites, while no significant difference was detected in non-infected mice, which indicated lung EVs are not factors to directly induce neutrophil recruitment but enhance neutrophil motor ability in response to inflammatory signal. Furthermore, inhibition of endogenous lung EV secretion by nasal instillation of GW4869 is sufficient to impair chemokine production and to reduce neutrophil chemotactic response. These findings suggest that the enhancement of neutrophil chemotaxis by lung EVs is different from inflammatory response to high-dose injection of proteins or nucleic acids.

Mantel-Cox test (****, $P < 0.0001$). (h) Absolute quantification of *S. typhimurium* DNA in peripheral blood 12 h post infection were detected by Real-time PCR (mean ± SEM; $n = 6$). Statistics by two-tailed unpaired Student's t test (*, $P < 0.05$). (i) Mouse survival curves post *S. typhimurium* infection. DMSO treated mice and GW4869 treated mice were inoculated intraperitoneally with 1×10^7 CFU/mouse bacteria in i, j ($n = 15$). Statistics by Mantel-Cox test (***, $P < 0.001$). (j) Absolute quantification of *S. typhimurium* DNA in peripheral blood 12 h post infection were detected by Real-time PCR (mean ± SEM; $n = 6$). Statistics by two-tailed unpaired Student's t test (*, $P < 0.05$). (k) Schema depicting regulations of lung EVs on bone marrow neutrophils

To examine the role of lung EVs in clinical diseases, we confirmed that the regulatory mechanisms identified in the present work are also functional during *Salmonella* infection. DNA in lung EVs is significantly increased during the early phase of acute inflammation induced by LPS and bacteria. Moreover, lung EVs promote neutrophil recruitment and finally effectively prolong the survival time of mice experienced acute infection. Consequently, lung EVs are a potential target for modulating neutrophil recruitment and chemokine release under various inflammatory stresses.

There are several limitations of our models. Although we demonstrated lung EVs transfer into blood, we cannot accurately quantify lung EVs in the circulation. GW4869 can effectively inhibit lung EVs secretion in vivo through nasal instillation. However, considering other unknown effects of GW4869, new techniques and models need to be established to remove or reduce endogenous EVs in tissues. Furthermore, there are differences between animal models and real conditions in vivo under physiological or pathological processes. Considering the rapid and unpredictable feature of infection progression, pre-treatment of lung EVs is not applicable to the real clinical situations. However, our conclusions suggest that further research could possibly encourage the development of novel EV-stimulators that upregulate secretion of endogenous lung EVs, providing additional therapeutic options for infectious diseases. It would also be helpful to synthesize lung EV-like vesicles in vitro, which might solve the ethical issues of EV source.

In summary, we have developed and validated a rigorous protocol for isolation of EVs from lung tissue that has allowed precise determination of their molecular composition and investigation of their physiological functions in vivo. The methodological framework provided here is a step toward a better understanding of vesicle-mediated long distance inter-organ communication. It also will be of importance to further investigate the pathological lung EVs released in disease for their future therapeutic potential and design of treatment interventions.

5 | GEOLOCATION INFORMATION

Peking University Health Science Center, 38 Xueyuan Road, Haidian, Beijing 100191, China.

AUTHOR CONTRIBUTIONS

B. Liu designed and performed the experiments, analysed data and wrote the manuscript. Y. Jin performed experiments and participated in the writing of the manuscript. J. Yang revised the manuscript. Y. Han helped with some experiments. H. Shan and X. Zhao did mass spectrometry analysis. M. Qiu provided clinical materials. A. Liu performed some bioinformatics analysis. Y. Jin supervised the experiments. Y. Yin conceived this research, supervised the experiments and wrote the manuscript.

COMPETING INTERESTS

The authors declare no competing interests.

DATA AVAILABILITY STATEMENT

The data and materials that support the findings of this study are available from the corresponding author upon reasonable request. The RNA-seq data in this study have been deposited in the SRA database with the accession code PRJNA776663. All pertinent information of our experiments has been submitted to the EV-TRACK knowledgebase (Consortium et al., 2017) (EV-TRACK ID: EV220127).

ETHICS APPROVAL STATEMENT

All procedures of human samples were conducted under the approval of the Ethics Committee of Peking University People's Hospital (Number 2021PHB118-001), and informed patient consent was obtained from all subjects in advance of sample collection. All procedures of laboratory animals were approved and monitored by the Animal Care and Use Committee of Peking University.

ORCID

Bowen Liu https://orcid.org/0000-0002-9310-8146
Yuan Jin https://orcid.org/0000-0001-6994-4892

REFERENCES

Ahmad-Nejad, P., Häcker, H., Rutz, M., Bauer, S., Vabulas, R. M., & Wagner, H. (2002). Bacterial CpG-DNA and lipopolysaccharides activate Toll-like receptors at distinct cellular compartments. *European Journal of Immunology*, *32*, 1958–1968. https://doi.org/10.1002/1521-4141(200207)32:7<1958::AID-IMMU1958>3.0.CO;2-U

Aliotta, J. M., Pereira, M., Li, M., Amaral, A., Sorokina, A., Dooner, M. S., Sears, E. H., Brilliant, K., Ramratnam, B., Hixson, D. C., & Quesenberry, P. J. (2012). Stable cell fate changes in marrow cells induced by lung-derived microvesicles. *Journal of Extracellular Vesicles*, *1*, https://doi.org/10.3402/jev.v1i0.18163

Aliotta, J. M., Pereira, M., Sears, E. H., Dooner, M. S., Wen, S., Goldberg, L. R., & Quesenberry, P. J. (2015). Lung-derived exosome uptake into and epigenetic modulation of marrow progenitor/stem and differentiated cells. *Journal of Extracellular Vesicles*, *4*, 26166, https://doi.org/10.3402/jev.v4.26166

Andaloussi, S. E., Mager, I., Breakefield, X. O., & Wood, M. J. (2013). Extracellular vesicles: Biology and emerging therapeutic opportunities. *Nature Reviews Drugs Discovery*, *12*, 347–357. https://doi.org/10.1038/nrd3978

Balaj, L., Lessard, R., Dai, L., Cho, Y. -. J., Pomeroy, S. L., Breakefield, X. O., & Skog, J. (2011). Tumour microvesicles contain retrotransposon elements and amplified oncogene sequences. *Nature Communication*, *2*, 180, https://doi.org/10.1038/ncomms1180

Bastarache, J. A., Fremont, R. D., Kropski, J. A., Bossert, F. R., & Ware, L. B. (2009). Procoagulant alveolar microparticles in the lungs of patients with acute respiratory distress syndrome. *American Journal of Physiology. Lung Cellular and Molecular Physiology*, *297*, L1035–L1041. https://doi.org/10.1152/ajplung.00214.2009

Bolger, A. M., Lohse, M., & Usadel, B. (2014). Trimmomatic: A flexible trimmer for Illumina sequence data. *Bioinformatics*, *30*, 2114–2120. https://doi.org/10.1093/bioinformatics/btu170

Burdon, P. C., Martin, C., & Rankin, S. M. (2005). The CXC chemokine MIP-2 stimulates neutrophil mobilization from the rat bone marrow in a CD49d-dependent manner. *Blood*, *105*, 2543–2548. https://doi.org/10.1182/blood-2004-08-3193

Consortium, E. -. T., Van Deun, J., Mestdagh, P., Agostinis, P., Akay, Ö., Anand, S., Anckaert, J., Martinez, Z. A., Baetens, T., Begkein, E., Bertier, L., Berx, G., Boere, J., Boukouris, S., Bremer, M., Buschmann, D., Byrd, J. B., Casert, C., Cheng, L., … Hendrix, A. (2017). EV-TRACK: Transparent reporting and centralizing knowledge in extracellular vesicle research. *Nature Methods*, *14*, 228–232. https://doi.org/10.1038/nmeth.4185

Crescitelli, R., Lasser, C., & Lotvall, J. (2021). Isolation and characterization of extracellular vesicle subpopulations from tissues. *Nature Protocols*, *16*(3), 1548–1580. https://doi.org/10.1038/s41596-020-00466-1

Danecek, P., Bonfield, J. K., Liddle, J., Marshall, J., Ohan, V., Pollard, M. O., Whitwham, A., Keane, T., Mccarthy, S. A., Davies, R. M., & Li, H. (2021). Twelve years of SAMtools and BCFtools. *Gigascience*, *10*, https://doi.org/10.1093/gigascience/giab008

Diamond, J. M., Vanpouille-Box, C., Spada, S., Rudqvist, N. -. P., Chapman, J. R., Ueberheide, B. M., Pilones, K. A., Sarfraz, Y., Formenti, S. C., & Demaria, S. (2018). Exosomes shuttle TREX1-sensitive IFN-stimulatory dsDNA from irradiated cancer cells to DCs. *Cancer Immunology Research*, *6*, 910–920. https://doi.org/10.1158/2326-6066.CIR-17-0581

Enaud, R., Prevel, R., Ciarlo, E., Beaufils, F., Wieërs, G., Guery, B., & Delhaes, L. (2020). The gut-lung axis in health and respiratory diseases: A place for inter-organ and inter-kingdom crosstalks. *Frontiers in Cellular and Infection Microbiology*, *10*, 9, https://doi.org/10.3389/fcimb.2020.00009

Engblom, C., Pfirschke, C., Zilionis, R., Martins, J. D. S., Bos, S. A., Courties, G., Rickelt, S., Severe, N., Baryawno, N., Faget, J., Savova, V., Zemmour, D., Kline, J., Siwicki, M., Garris, C., Pucci, F., Liao, H. -. W., Lin, Y. -. J., Newton, A., … Pittet, M. J. (2017). Osteoblasts remotely supply lung tumours with cancer-promoting SiglecF(high) neutrophils. *Science*, *358*, https://doi.org/10.1126/science.aal5081

Faubel, S., & Edelstein, C. L. (2016). Mechanisms and mediators of lung injury after acute kidney injury. *Nature Reviews Nephrology*, *12*, 48–60. https://doi.org/10.1038/nrneph.2015.158

Gardiner, C., Vizio, D. D., Sahoo, S., Théry, C., Witwer, K. W., Wauben, M., & Hill, A. F. (2016). Techniques used for the isolation and characterization of extracellular vesicles: Results of a worldwide survey. *Journal of Extracellular Vesicles*, *5*, 32945, https://doi.org/10.3402/jev.v5.32945

Gereke, M., Autengruber, A., Gröbe, L., Jeron, A., Bruder, D., & Stegemann-Koniszewski, S. (2012). Flow cytometric isolation of primary murine type II alveolar epithelial cells for functional and molecular studies. *Journal of Visualized Experiments: JoVE*, https://doi.org/10.3791/4322

Girbl, T., Lenn, T., Perez, L., Rolas, L., Barkaway, A., Thiriot, A., Fresno, C. D., Lynam, E., Hub, E., Thelen, M., Graham, G., Alon, R., Sancho, D., von Andrian, U. H., Voisin, M. -. B., Rot, A., & Nourshargh, S. (2018). Distinct compartmentalization of the chemokines CXCL1 and CXCL2 and the atypical receptor ACKR1 determine discrete stages of neutrophil diapedesis. *Immunity*, *49*, 1062–1076. e1066 https://doi.org/10.1016/j.immuni.2018.09.018

Haque, A., Engel, J., Teichmann, S. A., & Lonnberg, T. (2017). A practical guide to single-cell RNA-sequencing for biomedical research and clinical applications. *Genome Medicine*, *9*, 75, https://doi.org/10.1186/s13073-017-0467-4

Hemmi, H., Takeuchi, O., Kawai, T., Kaisho, T., Sato, S., Sanjo, H., Matsumoto, M., Hoshino, K., Wagner, H., Takeda, K., & Akira, S. (2000). A Toll-like receptor recognizes bacterial DNA. *Nature*, *408*, 740–745. https://doi.org/10.1038/35047123

Herrlich, A. (2021). Interorgan crosstalk mechanisms in disease: the case of acute kidney injury-induced remote lung injury. *Febs Letters*, https://doi.org/10.1002/1873-3468.14262

Hicks, S. C., Townes, F. W., Teng, M., & Irizarry, R. A. (2018). Missing data and technical variability in single-cell RNA-sequencing experiments. *Biostatistics (Oxford, England)*, *19*, 562–578. https://doi.org/10.1093/biostatistics/kxx053

Hoshino, A., Kim, H. S., Bojmar, L., Gyan, K. E., Cioffi, M., Hernandez, J., Zambirinis, C. P., Rodrigues, G., Molina, H., Heissel, S., Mark, M. T., Steiner, L., Benito-Martin, A., Lucotti, S., Di Giannatale, A., Offer, K., Nakajima, M., Williams, C., Nogués, L., … Lyden, D. (2020). Extracellular vesicle and particle biomarkers define multiple human cancers. *Cell*, *182*, 1044–1061. e1018 https://doi.org/10.1016/j.cell.2020.07.009

Huang da, W., Sherman, B. T., & Lempicki, R. A. (2009). Systematic and integrative analysis of large gene lists using DAVID bioinformatics resources. *Nature Protocols*, *4*, 44–57. https://doi.org/10.1038/nprot.2008.211

Hwang, B., Lee, J. H., & Bang, D. (2018). Single-cell RNA sequencing technologies and bioinformatics pipelines. *Experimental & Molecular Medicine*, *50*, 1–14. https://doi.org/10.1038/s12276-018-0071-8

Jeppesen, D. K., Fenix, A. M., Franklin, J. L., Higginbotham, J. N., Zhang, Q., Zimmerman, L. J., Liebler, D. C., Ping, J., Liu, Q., Evans, R., Fissell, W. H., Patton, J. G., Rome, L. H., Burnette, D. T., & Coffey, R. J. (2019). Reassessment of exosome composition. *Cell*, *177*, 428–445. e418 https://doi.org/10.1016/j.cell.2019.02.029

Jiang, W., Ma, P., Deng, L., Liu, Z., Wang, X., Liu, X., & Long, G. (2020). Hepatitis A virus structural protein pX interacts with ALIX and promotes the secretion of virions and foreign proteins through exosome-like vesicles. *Journal of Extracellular Vesicles*, *9*, 1716513, https://doi.org/10.1080/20013078.2020.1716513

Kolodziejczyk, A. A., Kim, J. K., Svensson, V., Marioni, J. C., & Teichmann, S. A. (2015). The technology and biology of single-cell RNA sequencing. *Molecular Cell*, *58*, 610–620. https://doi.org/10.1016/j.molcel.2015.04.005

Kulshreshtha, A., Ahmad, T., Agrawal, A., & Ghosh, B. (2013). Proinflammatory role of epithelial cell-derived exosomes in allergic airway inflammation. *Journal of Allergy and Clinical Immunology*, *131*, 1194–1203. 1203 e1191-1114. https://doi.org/10.1016/j.jaci.2012.12.1565

Lamphier, M., Zheng, W., Latz, E., Spyvee, M., Hansen, H., Rose, J., Genest, M., Yang, H., Shaffer, C., Zhao, Y., Shen, Y., Liu, C., Liu, D., Mempel, T. R., Rowbottom, C., Chow, J., Twine, N. C., Yu, M., Gusovsky, F., & Ishizaka, S. T. (2014). Novel small molecule inhibitors of TLR7 and TLR9: Mechanism of action and efficacy in vivo. *Molecular Pharmacology*, *85*, 429–440. https://doi.org/10.1124/mol.113.089821

Latz, E., Schoenemeyer, A., Visintin, A., Fitzgerald, K. A., Monks, B. G., Knetter, C. F., Lien, E., Nilsen, N. J., Espevik, T., & Golenbock, D. T. (2004). TLR9 signals after translocating from the ER to CpG DNA in the lysosome. *Nature Immunology*, *5*, 190–198. https://doi.org/10.1038/ni1028

Leek, J. T., Scharpf, R. B., Bravo, H. C., Simcha, D., Langmead, B., Johnson, W. E., Geman, D., Baggerly, K., & Irizarry, R. A. (2010). Tackling the widespread and critical impact of batch effects in high-throughput data. *Nature Reviews Genetics*, *11*, 733–739. https://doi.org/10.1038/nrg2825

Leifer, C. A., Kennedy, M. N., Mazzoni, A., Lee, C., Kruhlak, M. J., & Segal, D. M. (2004). TLR9 is localized in the endoplasmic reticulum prior to stimulation. *Journal of Immunology*, *173*, 1179–1183. https://doi.org/10.4049/jimmunol.173.2.1179

Li, H., & Durbin, R. (2009). Fast and accurate short read alignment with Burrows-Wheeler transform. *Bioinformatics*, *25*, 1754–1760. https://doi.org/10.1093/bioinformatics/btp324

Li, J., Liu, K., Liu, Y., Xu, Y., Zhang, F., Yang, H., Liu, J., Pan, T., Chen, J., Wu, M., Zhou, X., & Yuan, Z. (2013). Exosomes mediate the cell-to-cell transmission of IFN-alpha-induced antiviral activity. *Nature Immunology*, *14*, 793–803. https://doi.org/10.1038/ni.2647

Li, S. R., Man, Q. -W., Gao, X., Lin, H., Wang, J., Su, F. -C., Wang, H. -Q., Bu, L. -L., Liu, B., & Chen, G. (2021). Tissue-derived extracellular vesicles in cancers and non-cancer diseases: Present and future. *Journal of Extracellular Vesicles*, *10*, e12175, https://doi.org/10.1002/jev2.12175

Li, Y., Jin, Y., Liu, B., Lu, D., Zhu, M., Jin, Y., Mcnutt, M. A., & Yin, Y. (2019). PTENalpha promotes neutrophil chemotaxis through regulation of cell deformability. *Blood*, *133*, 2079–2089. https://doi.org/10.1182/blood-2019-01-899864

Lima, L. G., Chammas, R., Monteiro, R. Q., Moreira, M. E., & Barcinski, M. A. (2009). Tumour-derived microvesicles modulate the establishment of metastatic melanoma in a phosphatidylserine-dependent manner. *Cancer Letters*, *283*, 168–175. https://doi.org/10.1016/j.canlet.2009.03.041

Lötvall, J., Hill, A. F., Hochberg, F., Buzás, E. I., Di Vizio, D., Gardiner, C., Gho, Y. S., Kurochkin, I. V., Mathivanan, S., Quesenberry, P., Sahoo, S., Tahara, H., Wauben, M. H., Witwer, K. W., & Théry, C. (2014). Minimal experimental requirements for definition of extracellular vesicles and their functions: A position statement from the International Society for Extracellular Vesicles. *J Extracell Vesicles*, *3*, 26913, https://doi.org/10.3402/jev.v3.26913

Lu, D., Liu, L., Ji, X., Gao, Y., Chen, X., Liu, Y., Liu, Y., Zhao, X., Li, Y., Li, Y., Jin, Y., Zhang, Y., Mcnutt, M. A., & Yin, Y. (2015). The phosphatase DUSP2 controls the activity of the transcription activator STAT3 and regulates TH17 differentiation. *Nature Immunology*, *16*, 1263–1273. https://doi.org/10.1038/ni.3278

Marinov, G. K., Williams, B. A., McCue, K., Schroth, G. P., Gertz, J., Myers, R. M., & Wold, B. J. (2014). From single-cell to cell-pool transcriptomes: Stochasticity in gene expression and RNA splicing. *Genome Research*, *24*, 496–510. https://doi.org/10.1101/gr.161034.113

Merk, V. M., Phan, T. S., & Brunner, T. (2021). Regulation of tissue immune responses by local glucocorticoids at epithelial barriers and their impact on interorgan crosstalk. *Frontiers in Immunology*, *12*, 672808, https://doi.org/10.3389/fimmu.2021.672808

Mootha, V. K., Lindgren, C. M., Eriksson, K. -. F., Subramanian, A., Sihag, S., Lehar, J., Puigserver, P., Carlsson, E., Ridderstråle, M., Laurila, E., Houstis, N., Daly, M. J., Patterson, N., Mesirov, J. P., Golub, T. R., Tamayo, P., Spiegelman, B., Lander, E. S., Hirschhorn, J. N., … Groop, L. C. (2003). PGC-1alpha-responsive genes involved in oxidative phosphorylation are coordinately downregulated in human diabetes. *Nature Genetics*, *34*, 267–273. https://doi.org/10.1038/ng1180

Raredon, M. S. B., Adams, T. S., Suhail, Y., Schupp, J. C., Poli, S., Neumark, N., Leiby, K. L., Greaney, A. M., Yuan, Y., Horien, C., Linderman, G., Engler, A. J., Boffa, D. J., Kluger, Y., Rosas, I. O., Levchenko, A., Kaminski, N., & Niklason, L. E. (2019). Single-cell connectomic analysis of adult mammalian lungs. *Science Advances*, *5*, eaaw3851, https://doi.org/10.1126/sciadv.aaw3851

Sansone, P., Savini, C., Kurelac, I., Chang, Q., Amato, L. B., Strillacci, A., Stepanova, A., Iommarini, L., Mastroleo, C., Daly, L., Galkin, A., Thakur, B. K., Soplop, N., Uryu, K., Hoshino, A., Norton, L., Bonafé, M., Cricca, M., … Bromberg, J. (2017). Packaging and transfer of mitochondrial DNA via exosomes regulate escape from dormancy in hormonal therapy-resistant breast cancer. *PNAS*, *114*, E9066–E9075. https://doi.org/10.1073/pnas.1704862114

Sarkar, A., & Stephens, M. (2021). Separating measurement and expression models clarifies confusion in single-cell RNA sequencing analysis. *Nature Genetics*, *53*, 770–777. https://doi.org/10.1038/s41588-021-00873-4

Shao, H., Im, H., Castro, C. M., Breakefield, X., Weissleder, R., & Lee, H. (2018). New technologies for analysis of extracellular vesicles. *Chemical Review*, *118*, 1917–1950. https://doi.org/10.1021/acs.chemrev.7b00534

Shashaty, M. G. S., Forker, C. M., Miano, T. A., Wu, Q., Yang, W., Oyster, M. L., Porteous, M. K., Cantu, E. E., Diamond, J. M., & Christie, J. D. (2019). The association of post-lung transplant acute kidney injury with mortality is independent of primary graft dysfunction: A cohort study. *Clinical Transplantation*, *33*, e13678, https://doi.org/10.1111/ctr.13678

Skotland, T., Sandvig, K., & Llorente, A. (2017). Lipids in exosomes: Current knowledge and the way forward. *Progress in Lipid Research*, *66*, 30–41. https://doi.org/10.1016/j.plipres.2017.03.001

Stunz, L. L., Lenert, P., Peckham, D., Yi, A. -. K., Haxhinasto, S., Chang, M., Krieg, A. M., & Ashman, R. F. (2002). Inhibitory oligonucleotides specifically block effects of stimulatory CpG oligonucleotides in B cells. *European Journal of Immunology*, *32*, 1212–1222. https://doi.org/10.1002/1521-4141(200205)32:5<1212::AID-IMMU1212>3.0.CO;2-D

Subramanian, A., Tamayo, P., Mootha, V. K., Mukherjee, S., Ebert, B. L., Gillette, M. A., Paulovich, A., Pomeroy, S. L., Golub, T. R., Lander, E. S., & Mesirov, J. P. (2005). Gene set enrichment analysis: a knowledge-based approach for interpreting genome-wide expression profiles. *PNAS*, *102*, 15545–15550. https://doi.org/10.1073/pnas.0506580102

Svensson, V., Natarajan, K. N., Ly, L. -. H., Miragaia, R. J., Labalette, C., Macaulay, I. C., Cvejic, A., & Teichmann, S. A. (2017). Power analysis of single-cell RNA-sequencing experiments. *Nature Methods*, *14*, 381–387. https://doi.org/10.1038/nmeth.4220

Takahashi, A., Okada, R., Nagao, K., Kawamata, Y., Hanyu, A., Yoshimoto, S., Takasugi, M., Watanabe, S., Kanemaki, M. T., Obuse, C., & Hara, E. (2017). Exosomes maintain cellular homeostasis by excreting harmful DNA from cells. *Nature Communication*, *8*, 15287, https://doi.org/10.1038/ncomms15287

Talevich, E., Shain, A. H., Botton, T., & Bastian, B. (2016). Genome-wide copy number detection and visualization from targeted DNA sequencing. *Plos Computational Biology*, *12*, e1004873, https://doi.org/10.1371/journal.pcbi.1004873

Thakur, B. K., Zhang, H., Becker, A., Matei, I., Huang, Y., Costa-Silva, B., Zheng, Y., Hoshino, A., Brazier, H., Xiang, J., Williams, C., Rodriguez-Barrueco, R., Silva, J. M., Zhang, W., Hearn, S., Elemento, O., Paknejad, N., Manova-Todorova, K., Welte, K., … Lyden, D. (2014). Double-stranded DNA in exosomes: A novel biomarker in cancer detection. *Cell Research*, *24*, 766–769. https://doi.org/10.1038/cr.2014.44

Tkach, M., & Thery, C. (2016). Communication by extracellular vesicles: Where we are and where we need to go. *Cell*, *164*, 1226–1232. https://doi.org/10.1016/j.cell.2016.01.043

Trajkovic, K., Hsu, C., Chiantia, S., Rajendran, L., Wenzel, D., Wieland, F., Schwille, P., Brügger, B., & Simons, M. (2008). Ceramide triggers budding of exosome vesicles into multivesicular endosomes. *Science*, *319*, 1244–1247. https://doi.org/10.1126/science.1153124

Verweij, F. J., Revenu, C., Arras, G., Dingli, F., Loew, D., Pegtel, D. M., Follain, G., Allio, G., Goetz, J. G., Zimmermann, P., Herbomel, P., Bene, F. D., Raposo, G., & van Niel, G. (2019). Live tracking of inter-organ communication by endogenous exosomes in vivo. *Developmental Cell*, *48*, 573–589. e574 https://doi.org/10.1016/j.devcel.2019.01.004

Wang, L., Li, Y., Guan, X., Zhao, J., Shen, L., & Liu, J. (2018). Exosomal double-stranded DNA as a biomarker for the diagnosis and preoperative assessment of pheochromocytoma and paraganglioma. *Molecular Cancer*, *17*, 128, https://doi.org/10.1186/s12943-018-0876-z

Yang, L., Liu, Q., Zhang, X., Liu, X., Zhou, B., Chen, J., Huang, D., Li, J., Li, H., Chen, F., Liu, J., Xing, Y., Chen, X., Su, S., & Song, E. (2020). DNA of neutrophil extracellular traps promotes cancer metastasis via CCDC25. *Nature*, *583*, 133–138. https://doi.org/10.1038/s41586-020-2394-6

Yang, L., Peng, X., Li, Y., Zhang, X., Ma, Y., Wu, C., Fan, Q., Wei, S., Li, H., & Liu, J. (2019). Long non-coding RNA HOTAIR promotes exosome secretion by regulating RAB35 and SNAP23 in hepatocellular carcinoma. *Molecular Cancer*, *18*, 78, https://doi.org/10.1186/s12943-019-0990-6

Yokoi, A., Villar-Prados, A., Oliphint, P. A., Zhang, J., Song, X., De Hoff, P., Morey, R., Liu, J., Roszik, J., Clise-Dwyer, K., Burks, J. K., O'halloran, T. J., Laurent, L. C., & Sood, A. K. (2019). Mechanisms of nuclear content loading to exosomes. *Science Advances*, *5*, eaax8849, https://doi.org/10.1126/sciadv.aax8849

Zhang, L., Li, Z., Skrzypczynska, K. M., Fang, Q., Zhang, W., O'brien, S. A., He, Y., Wang, L., Zhang, Q., Kim, A., Gao, R., Orf, J., Wang, T., Sawant, D., Kang, J., Bhatt, D., Lu, D., Li, C. -. M., Rapaport, A. S., … Yu, X. (2020). Single-cell analyses inform mechanisms of myeloid-targeted therapies in colon cancer. *Cell*, *181*, 442–459. e429 https://doi.org/10.1016/j.cell.2020.03.048

Zhang, Q., Raoof, M., Chen, Y., Sumi, Y., Sursal, T., Junger, W., Brohi, K., Itagaki, K., & Hauser, C. J. (2010). Circulating mitochondrial DAMPs cause inflammatory responses to injury. *Nature*, *464*, 104–107. https://doi.org/10.1038/nature08780

Zhao, M., Liu, S., Wang, C., Wang, Y., Wan, M., Liu, F., Gong, M., Yuan, Y., Chen, Y., Cheng, J., Lu, Y., & Liu, J. (2021). Mesenchymal stem cell-derived extracellular vesicles attenuate mitochondrial damage and inflammation by stabilizing mitochondrial DNA. *ACS Nano*, *15*, 1519–1538. https://doi.org/10.1021/acsnano.0c08947

Zomer, A., Maynard, C., Verweij, F. J., Kamermans, A., Schäfer, R., Beerling, E., Schiffelers, R. M., De Wit, E., Berenguer, J., Ellenbroek, S. I. J., Wurdinger, T., Pegtel, D. M., & Van Rheenen, J. (2015). In vivo imaging reveals extracellular vesicle-mediated phenocopying of metastatic behavior. *Cell*, *161*, 1046–1057. https://doi.org/10.1016/j.cell.2015.04.042

SUPPORTING INFORMATION

Additional supporting information can be found online in the Supporting Information section at the end of this article.